Scanning Microscopy

Volume 4 | Number 3 Article 3

8-27-1990

Surface Diffusion Studies by Analysis of Cluster Growth Kinetics

Martin Zinke-Allmang
Research Centre Jülich

Scanning Microscopy, Vol. 4, No. 3, 1990 (Pages 523-542)
Scanning Microscopy International, Chicago (AMF O'Hare), IL 60666 USA

0891-7035/90$3.00+.00

SURFACE DIFFUSION STUDIES BY ANALYSIS OF CLUSTER GROWTH KINETICS

Martin Zinke-Allmang*

Institute of Thin Film and Ion Technology, Research Centre Jülich
P.O. Box 1913, 5170 Jülich, F.R.G.

(Received for publication March 8, 1990, and in revised form August 27, 1990)

Abstract

The approach to thermodynamic equilibrium is the driving force for kinetic processes in adsorbate and thin film structure formation. Macroscopic thermodynamic concepts may be used to predict the rates of nucleation, cluster formation and cluster growth. They involve mass transport concepts usually limited by surface concentration gradients. Time and temperature dependence of nucleation and cluster growth, described in terms of cluster ripening mechanism, therefore reveal information on the microscopic surface diffusion processes, including surface structure and surface energies. Examples of structures studied include, Ga, Sn, and Ge on Si, As terminated Si and GaAs surfaces where the activation energies for clustering are obtained without using laterally resolved techniques requiring μm-patch deposition. The results are in agreement with activation energies found in nucleation experiments of Ag on Si.

The concentration dependence of the surface diffusion coefficient in clustering systems is connected to the difference between the intrinsic diffusion coefficient and the chemical or mass transport diffusion coefficient. The difference results from the analysis of an extended Einstein relation for diffusion in these systems. The intrinsic diffusion coefficient of Sn and Ga on Si is concentration independent in cluster growth experiments. Literature data for surface diffusion of Ag/Ge(111) and O/W(110) show a concentration dependence which is in good agreement with the dependence predicted for the chemical diffusion coefficient by this model.

Key Words: surface diffusion, cluster formation, nucleation, cluster growth, Ostwald ripening, ion scattering analysis, reflection electron microscopy, scanning Auger microscopy, semiconductor heterosystems, Stranski-Krastanov and Volmer-Weber growth model, epitaxy.

* Address for correspondence:
M. Zinke-Allmang, Research Centre Jülich, Institute of Thin Film and Ion Technology, P.O. Box 1913, D-5170 Jülich, F.R.G.

Phone No. +49(2461)613715

Introduction

The knowledge of surface diffusion parameters is crucial in the interpretation of a large number of processes at surfaces. Among these are issues of fundamental interest such as the kinetics of first order phase transitions, as well as important applied technologies like catalytic reactions, corrosion effects and thin film growth. The special interest in surface diffusion coefficients in the latter technology has recently been addressed in a materials science panel report on "Fundamental issues in Heteroepitaxy" [4].

Despite this important role of surface diffusion, systematic studies are still limited to a few systems. Theoretical models which allow one to predict diffusion coefficients for previously not investigated surface/adsorbate systems do not exist. This is mainly due to the complexity of the problem; contrary to bulk diffusion studies, technical requirements for reproducible surface diffusion experiments are high. They include properly cleaned and characterized surfaces under ultra high vacuum or ultra pure conditions and in-situ deposition and characterization techniques to follow the diffusion process.

In addition, strong dependences on the substrate surface orientation and the concentration of the adsorbate are expected. Varying diffusion coefficients on different crystal planes, e.g. (100) and (111) faces of cubic crystals, are discussed in the experimental section. Also directional dependences on a particular plane occur as theoretically discussed by Stoyanov [48] for the symmetry breaking 2x1 reconstruction of Si(100) surfaces. These predictions are supported by recent STM measurements of homoepitaxial growth of Si on Si(100) [33, 34]. Variations of diffusion coefficients as a function of adsorbate concentration surely exist. E.g. our data for Ge on Si diffusion are measured for Ge on a completed uniform layer of Ge (Stranski-Krastanov layer [2, 3]). The data presented by Gossmann and Fisanick in this volume [25] describe the diffusion of Ge on bare Si surfaces during the formation of this uniform Ge by in-situ scanning electron microscopy (SEM) and scanning Auger microscopy (SAM).

In this review we describe first the significant role of surface diffusion in cluster formation (nucleation) and cluster growth on surfaces. Experimental data based on these models are summarized. Following an introduction of the experimental methods with an emphasis on ion scattering techniques,

Table 1: List of symbols.

a	substrate lattice constant
b_j	number of bonds in cluster with j atoms
$c(r)$	adatom concentration in equilibrium with cluster of radius r (Gibbs–Thomson equation)
c_∞	equilibrium adatom concentration (solubility) of large clusters
c_{free}	free adatom concentration in equilibrium with cluster size distribution
$c'(r)$	actual concentration of adatoms at cluster surface
c_C	concentration of adatoms in a cluster
c_t	concentration of adatoms in excess of Stranski–Krastanov layer
D_s	intrinsic surface diffusion coefficient
D_a	chemical or mass transport surface diffusion coefficient
dn_D/dt	amount of material exchange for diffusion limited mass transport
dn_T/dt	amount of material exchange for interface transfer limited mass transport
E_a	activation energy of reevaporation
E_b	bond energy adatom–adatom
E_c	activation energy of cluster growth
E_d	activation energy of diffusion
E_f	free enthalpy of cluster formation
E_s	bond energy adatom–substrate
$F(r)$	total Gibbs free energy of a cluster of radius r
$f(r,t)$	cluster size distribution on the surface
h_C	average cluster height as obtained from ion scattering experiment
i^*	number of atoms in critical cluster in nucleation experiments
J	nucleation rate
j_x	average number of atoms in stable clusters in nucleation experiments
l_{sc}	screening length factor used as boundary condition for Fick's second law of diffusion on a surface
N	number of atoms in an adlayer structure
$N(j)$	number of clusters with j atoms per unit area
N_s	number of available sites on the substrate surface
N_x	number of stable clusters per unit area in nucleation experiments
p_o	equivalent pressure of adatoms on the surface under standard thermodynamic conditions
p_{eq}	equivalent equilibrium pressure of clustered system
P_i	probability for adatom to be in i^{th} surface state
R	deposition rate
r_c	radius of cluster in equilibrium with free adatom concentration at time t
r_k	radius of critical cluster, i.e. cluster which becomes stable upon addition of a further atom
$S_{av}(r)$	total surface adatoms/vacuum per unit area
$S_{as}(r)$	total surface adatoms/substrate per unit area
$S_{sv}(r)$	total surface substrate/vacuum per unit area
S_T	surface of cluster active in interface transfer mass transport
S_C	surface of a cluster
S_m^s	entropy of migration of single atoms on the surface
$V_C(r)$	volume of a cluster of radius r
v_M^C	atomic volume of cluster material
v_M^{free}	atomic volume of material in the free adatom concentration
W	relative interaction strength E_s/E_b
γ_{av}	surface tension of adatoms
γ_{as}	interface tension adatoms/substrate
γ_{sv}	surface tension of substrate
Θ	contact angle of cluster with substrate
κ_a	kinetic constant of interface mass transfer when the full surface of the cluster is active in the process
κ_r	kinetic constant of interface mass transfer when only the periphery line of the cluster is active in the process
Λ	diffusion length
μ_C	chemical potential of bulk cluster material
μ_{free}	chemical potential of free adatoms
ν_{as}	vibrational frequency of adatoms perpendicular to the substrate
$\rho_{in}(j)$	capture collision factor of cluster with j atoms
$\rho_{out}(j)$	collision factor for atoms leaving from a cluster with j atoms
τ_a	average time for reevaporation from surface
τ_c	time constant of cluster growth process
τ_d	average time for a single diffusion jump
τ_{free}	average time for adatoms to stay in free concentration
τ_i	average time for adatoms in i^{th} surface state
τ_m	average time for the arrival of a full monolayer equivalent coverage

which were only recently applied to cluster growth studies [66, 67, 69], results from the nucleation regime and the late stage growth regime are compared. In a final section the concentration dependence on adsorbate concentration [9, 10, 49] is discussed.

Clustering Kinetics: Basic Concepts

Three dimensional clusters and two dimensional islands on surfaces are widespread phenomena in fundamental and applied surface science studies.

In non–equilibrium thermodynamics investigating phase transitions and phase separation they serve as model systems [27] for the evolution of systems with a conserved order parameter [1], e.g. the concentration. A typical experiment is a quench from a one–phase equilibrium state into a two–phase coexistence regime of a two–dimensional adsorbate layer on a surface [52]. The central issues addressed in such studies are the description of the formation of the new phase and irreversible processes and rates during the evolution towards the new equilibrium state.

Clusters or islands play further a key role in properties

of applied systems like catalytic processes and in thin film growth by molecular beam epitaxy [66]. In such techniques the two phase coexistence regime is entered along isothermal lines. This allows one to include surface systems without a critical point like coexistence regimes of liquid–like and solid–like adsorbate phases. In these studies the major issues are the cluster influence on surface diffusion and desorption rates to minimize the degradation of the achieved structure.

The central relevance of cluster structures in adlayer systems is due to equilibrium thermodynamics comparing two– and three–dimensional aggregates to uniform layers. This is illustrated in Fig. 1. Plotted is the energy of a system as a function of the film thickness (in equivalent monolayer coverage) at zero temperature. The solid lines represent crystalline adlayers growing commensurate on the substrate [26]. Two cases are distinguished for the adlayer–substrate bond strength, E_s, relative to the adlayer–adlayer bond strength, E_b, $W = E_s/E_b$: for $W > 1$ the substrate interaction dominates (Stranski–Krastanov condition) and for $W < 1$ the adlayer interaction is stronger (Volmer–Weber condition) [2, 3]. Further a non–zero misfit between the substrate and adatom lattice is assumed. This introduces a strain energy in the film–like structure which increases with increasing film thickness.

The energy axis is given by (E(N) - E(0) - μ_{bulk} N) with μ_{bulk} the equivalent chemical potential of bulk material of the adlayer atoms. This choice illustrates best the approach of the growing adlayer towards bulk properties with the slope of the curve given by $(\partial E/\partial N) - \mu_{bulk} = \mu_{film} - \mu_{bulk}$ [26]. Both, two– and three–dimensional aggregation are predicted from Fig. 1 noting that the real system avoids upward slopes by phase separation.

Following the line for $W > 1$ a random completion of full layers would result in the shown oscillations. Unpaired bonds, edge– and corner–like arrangements result between full layers in an increase in energy. In the real system these oscillations are replaced by a common–tangent of both minima regions representing two–dimensional island formation. Thus the system crosses per layer grown a two phase coexistence regime and single phases occur only in a narrow range close to the minima of the energy curve at full layers. A transition to three–dimensional clustering occurs if the chemical potential μ_{film} exceeds μ_{bulk}, i.e. the slope of the common–tangent curve becomes positive.

In the case $W < 1$ the equilibrium configuration is given by three–dimensional clusters on the bare substrate since the slope of the curve is positive for all values of N [32].

The general conclusions from Fig. 1 remain unchanged for amorphous and liquid adsorbates [65]. Note that an ideal amorphous adlayer would yield the dashed–dotted lines implying for $W > 1$ uniform growth of the amorphous adlayer (Frank–van der Merwe condition) [2, 3]. The presence of the crystalline substrate, however, imposes a short range order in a realistic amorphous overlayer (dashed line).

This section contains a review of theoretical approaches to the kinetics of phase separation in such systems including the nucleation of a new phase under supersaturation and the growth of the cluster nuclei with the restriction to zero–deposition rate conditions. We emphasize especially the late stage regime since a complete analytical treatment exists.

Nucleation. The discussion of nucleation processes is based on three main models:

1. Nucleation rates based on bulk thermodynamic properties of the cluster material,

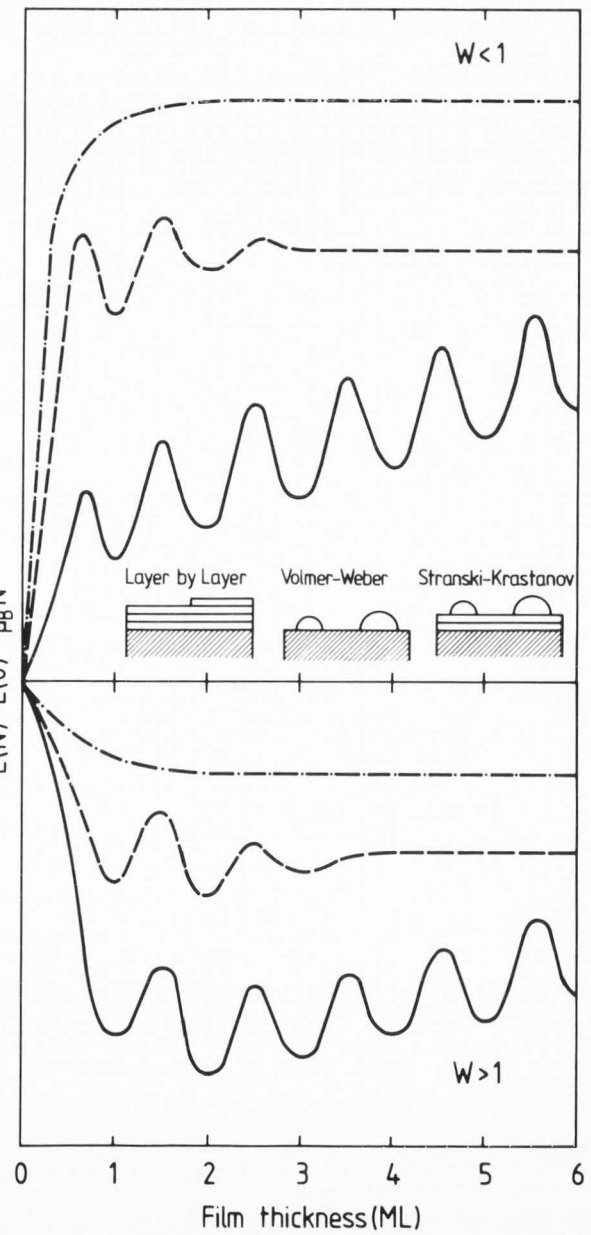

Fig.1. Energy relative to that of the bulk crystalline state, plotted versus the film thickness for a film–substrate interaction strength larger ($W > 1$) and smaller ($W < 1$) than the film–film interaction. Reprinted with permission from Ref. [26].

2. nucleation rates based on atomistic quantities assigned to cluster atoms,

3. kinetic rate equations which describe the change of number of clusters for each size j separately (with j the number of atoms in the cluster).

In the bulk thermodynamic limit the energetics of aggregations of atoms is described by the total Gibbs free energy [8, 58] in the form:

$$\mathbf{F(r)} = (\mu_C - \mu_{free})\ V_C(r)\left(\frac{1}{v_M^C} - \frac{1}{v_M^{free}}\right) + \ldots$$
$$\ldots + S_{av}(r)\gamma_{av} + S_{as}(r)\gamma_{as} + S_{sv}(r)\gamma_{sv} \qquad (1)$$

with μ the chemical potentials for bulk material in clusters (index C) and in the free adatom concentration (index free), v_M the atomic volumes and the surface terms S and surface tensions γ as defined by Fig. 2 [38] with index a for adatom, index s for substrate and index v for vacuum. V(r) is the volume of the cluster.

Eq.(1) contains a term which corresponds to the gain in total energy by increasing the volume of a cluster while the three surface terms correspond to an energy increase due to formation of new surfaces.

Assuming the free adatom concentration to be an ideal solution on the substrate surface allows one to simplify Eq.(1) using $(v_M^C)^{-1} \gg (v_M^{free})^{-1}$ and

$$\mu_C - \mu_{free} = \mu_{C,o}(T) - \mu_{free,o}(T) - kT\ln\left(\frac{p}{p_o}\right) \qquad (2)$$

with index o for standard conditions. Choosing $p_o = p_{eq}$, i.e. the equilibrium vapor pressure at temperature T, the first two terms in Eq.(2) are of equal magnitude. As Ostwald showed [42, 43] the term p/p_{eq} can be replaced by c/c_∞ with c the adatom concentration and c_∞ the equilibrium solubility of a very large cluster.

Using the condition $dF(r)/dr = 0$ in Eq.(1) allows one to determine c and r for a cluster for which the increasing surface energy and the decreasing volume free energy are just balanced.

If the clusters are in their equilibrium shape geometrical arguments and the Young-Dupré equation [38] allow one to combine the surface terms in Eq.(1) yielding the Gibbs–Thomson equation [22, 50, 51]:

$$\frac{kT}{v_M^C}\ln\left(\frac{p}{p_{eq}}\right) = \frac{2}{r}\gamma_{av} \qquad (3)$$

This equation can be used in two different ways for cluster growth problems:

1. In experiments with variable deposition rates, i.e. variable vapor pressures, p, the radius of the clusters with an equal probability to grow or decay, r_k, is determined:

$$r_k = \frac{2\gamma_{av}v_M^C}{kT}\left[\ln\left(\frac{p}{p_{eq}}\right)\right]^{-1} \qquad (4)$$

By adding one further atom to a cluster of "critical radius" the cluster becomes stable, i.e. it will not decay anymore. This equation applies to nucleation experiments.

2. For a given radius r the free concentration is calculated with the same probability for this cluster to grow or to decompose. Thus a concentration c(r) is obtained with which the cluster is in dynamic equilibrium:

$$c(r) = c_\infty \exp\left(\frac{2\gamma_{av}v_M^C}{rkT}\right) \qquad (5)$$

In this form the Gibbs–Thomson equation applies to cluster growth under zero deposition rate conditions as discussed in the second part of this section.

The nucleation rate of stable clusters is given by the areal density of critical clusters, $N(r_k)$, and the rate at which these clusters gain an additional atom:

$$J = N(r_k)N(1)\rho_{in}(r_k) \qquad (6)$$

where N(1) is the free concentration of monomers on the surface and $\rho_{in}(r_k)$[1] is a collision factor containing two contributions, direct impingement from the vapor phase and surface diffusion of monomers. Mobility of larger clusters [31] is

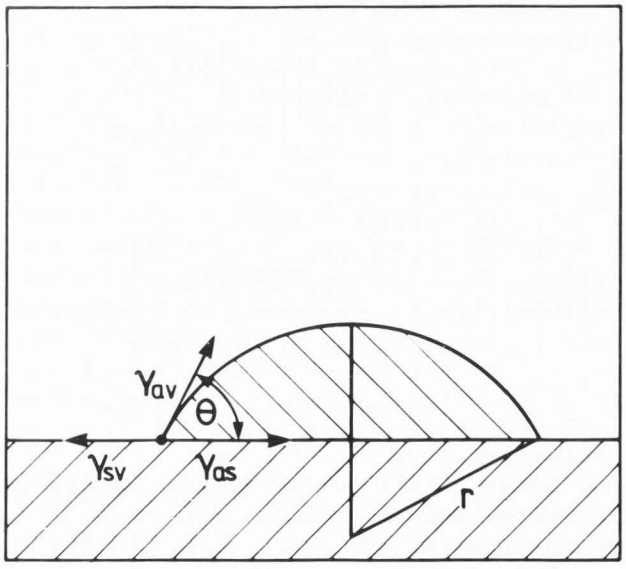

Fig.2. Partial spherical cluster of radius r and contact angle Θ on a surface. For clusters in their equilibrium shape the three tension terms, adatom–vacuum surface tension, γ_{av}, substrate–vacuum surface tension, γ_{sv}, and substrate–adatom interfacial tension, γ_{as}, are connected by the Young-Dupré equation [38].

[1] The notation in this paper differs from nucleation theory literature [19,54–56]. It is choosen to emphasize the explicit dependence on the number densities of clusters and monomers.

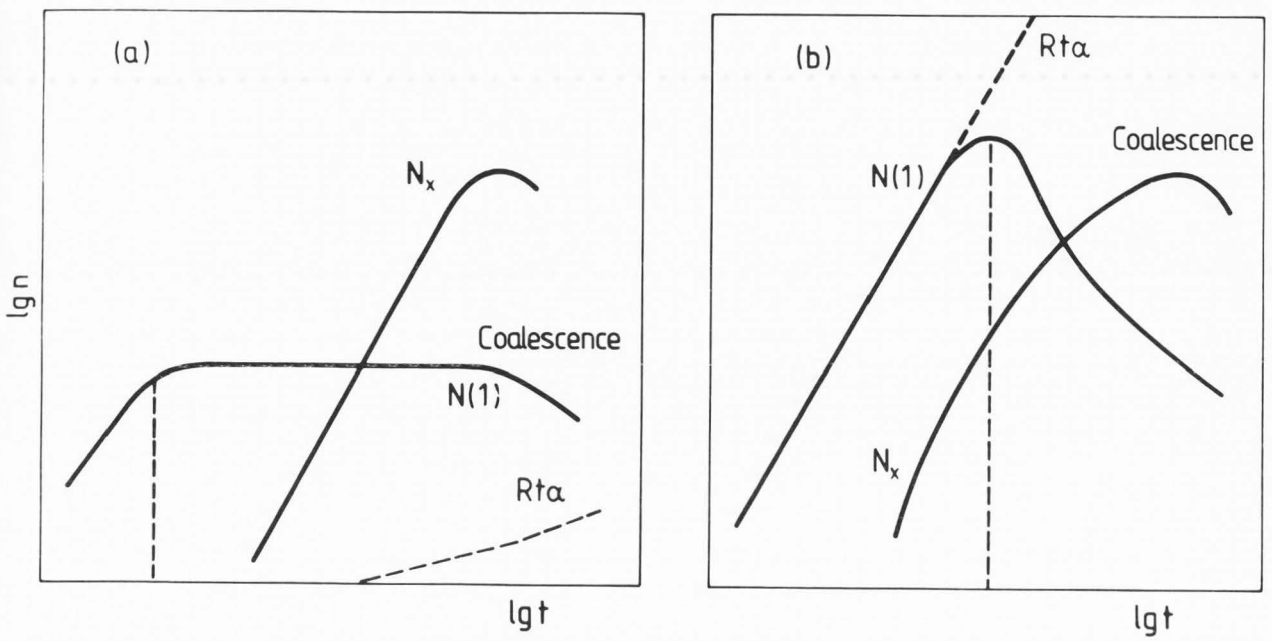

Fig.3. Time dependence of the monomer concentration, N(1), and the stable cluster density, N_x, as a function of deposition time for (a) high temperature and (b) low temperature. The transition from the initial stage to the steady–state regime is indicated by vertical dashed lines. Reprinted with permission from Ref. [57].

neglected and in most experimental cases the diffusion mechanism dominates [46]. Eq.(6) is achieved from the steady state model of nucleation developed by Becker and Döring [5] with continuous monomer supply to compensate for the loss of mass by removing stable clusters from the system [20]. Corrections for deviations from the equilibrium distribution are neglected [62]. This model is restrictive since the stable cluster phase cannot accumulate a finite area fraction on the surface.

The three factors in Eq.(6) introduce three activation energies governing the temperature dependence of J: $\rho_{in}(r_k)$ is determined by the activation energy of diffusion, E_d, N(1) is determined by the activation energy of desorption, E_a, based on the equilibrium between the desorption and the impingement flux, and $N(r_k)$ is determined by the energy of formation of a critical cluster, $F(r_k)$:

$$J = \text{const} \cdot p \cdot \exp\left[\frac{E_a - E_d - F(r_k)}{kT}\right] \qquad (7)$$

where p is the vapor pressure generated by the deposition process. A measurement of J as a function of temperature does not yield a simple Arrhenius plot since r_k and therefore $F(r_k)$ depend on temperature (Eq.(3)). The implications of this finding on the evaluation of surface diffusion data from nucleation experiments are discussed below based on a more detailed picture of the nucleation process.

Since critical clusters often contain only a few atoms [8] or even one atom [35] atomic quantities like binding energies of atoms at different sites on the substrate or at the cluster are used instead of the thermodynamic quantities [60]. If adsorption–desorption equilibrium is given, i.e. at high enough substrate temperatures, the Walton relation [60, 61] is valid, which still requires quasi equilibrium conditions and applies the law of mass action finding

$$\left(\frac{N(i^*)}{N_s}\right) = \left(\frac{N(1)}{N_s}\right)^{i^*} \exp\left[-\frac{E_{i^*}}{kT}\right] \qquad (8)$$

where i^* is the number of atoms in the critical cluster, E_{i^*} is the change in potential energy if a cluster with i^* atoms is formed from single atoms [61] and N_s is the number of adsorption sites on the substrate. Eq.(8) replaces Eq.(1) in the determination of the nucleation rate from Eq.(6):

$$J = RN_s a^2 \left(\frac{R}{\nu_{as} N_s}\right)^{i^*} \exp\left[\frac{(i^*+1)E_a - E_{i^*} - E_d}{kT}\right] \qquad (9)$$

where a is the substrate lattice constant, ν_{as} is the vibrational frequency and R is the condensation flux (dimension $cm^{-2}sec^{-1}$) used instead of the equivalent term in Eq.(7).

Both concepts for nucleation, the thermodynamic and the atomistic model, are restricted in their applications since [19]:

1. no spatial gradient of the free adatom concentration N(1) is considered as formed by diffusion processes on the surface,
2. clusters with $r > r_k$ are considered absolutely stable and clusters with $r \leq r_k$ are distributed as given by Eq.(8) (quasi–equilibrium condition) and

3. a steady state solution is assumed including all clusters up to the stable clusters.

These restrictions do not apply to a model based on kinetic rate equations. In these equations the change in number of j–sized clusters is written as a function of all microscopic atom capture and release processes [19, 54][2]:

$$\frac{dN(1)}{dt} = R - \frac{N(1)}{\tau_a} - N^2(1)\rho_{in}(1) + \ldots + \ldots + \sum_{j=2}^{\infty} [\rho_{out}(j) - N(1)\rho_{in}(j)]\, N(j) \qquad (10)$$

$$\frac{dN(2)}{dt} = N(1)\,[\rho_{in}(1)N(1) - \rho_{in}(2)N(2)] + \ldots + \ldots + [\rho_{out}(3)N(3) - \rho_{out}(2)N(2)] \qquad (11)$$

$$\vdots$$

$$\frac{dN(j)}{dt} = N(1)\,[\rho_{in}(j-1)N(j-1) - \rho_{in}(j)N(j)] + \ldots + \ldots + [\rho_{out}(j+1)N(j+1) - \rho_{out}(j)N(j)] \qquad (12)$$

$$\vdots$$

The first equation describes the change in number of single atoms N(1), i.e. changes in the free concentration. It contains the deposition rate, loss of atoms due to reevaporation with τ_a the average of stay on the surface, loss due to formation of dimers and due to capture of single atoms by bigger clusters and release of single atoms from a big cluster. Each of these rates is given by a product of the number of involved species and a collision factor depending on the size of the cluster. The second and all following equations represent the change in number of clusters with j atoms, losses due to capture or release of single atoms and gains due to growth of the next smaller cluster or decomposition of the next larger cluster. Note that mobility of larger clusters and coalescence, i.e. growth of entire clusters into each other, are neglected.

In order to use Eqs.(10) – (12) quantitatively, the collision factors ρ_{in} and ρ_{out} have to be specified. Restricting the discussion to diffusion limited mass transport ρ_{in} is given by [54]

$$\rho_{in} = 2\pi r \sin\Theta \, \frac{D_a}{N(1)} \left(\frac{\partial N(1)}{\partial r'} \right)\Bigg|_{r'=r\sin\Theta} \qquad (13)$$

where D_a is the surface diffusion coefficient.

Venables [19, 54] separated Eqs.(10) – (12) in three groups, an equation for single adatoms, equations for the non–stable clusters ($j \leq i^*$) and an equation combining all stable clusters [56]:

$$\frac{dN(1)}{dt} = R - \frac{N(1)}{\tau_a} - \frac{d(N_x j_x)}{dt} \qquad (14)$$

$$\frac{dN(j)}{dt} = 0 \qquad (15)$$

$$\frac{dN_x}{dt} = N(1)\rho_{in}(i^*)N(i^*) \qquad (16)$$

with $N_x j_x$ the total number of atoms in stable clusters. Eq.(16) is equal to the nucleation rate given in Eq.(6).

If coalescence terms are included in Eq.(16) Venables [54] showed that a maximum cluster density is reached. This quantity is easier to measure than nucleation rates (Fig. 3, [57]):

1. In an intital regime the deposition rate R dominates in Eq.(14) with N(1) = Rt. If this regime is limited by a small desorption time τ_a (high temperature, Fig. 3(a)), N_x is still very low at the end of this regime. At low temperatures, i.e. when evaporation from the surface is excluded, N(1) in Eq.(14) is limited by the term $d(N_x j_x)/dt$. This term is dominated by surface diffusion as the major contribution [57]. In this case at the end of the initial regime the number of stable clusters is already larger (Fig. 3(b)).

2. The following regime is characterized by steady state conditions for the concentration of single adatoms. In this regime the largest number of clusters is formed. In most experimental cases this regime is reached very quickly [31]. The dependence of the density of stable cluster, is given by

$$\frac{N_x}{N_s} \propto \left(\frac{R}{N_s \nu_{as}} \right)^q \exp\left[\frac{E}{kT} \right] \qquad (17)$$

where at low temperatures $q = 1/(i^* + d')$ and $E = (E_{i^*} + i^* E_d)/(i^* + d')$ with $d' = 2.5$ for three–dimensional clusters and $d' = 2$ for two–dimensional islands [54, 56].

Note that for the assumed complete condensation regime, i.e. when $\tau_a \gg \sqrt{\tau_m \tau_d}$ with τ_m the average time for the arrival of a full monolayer equivalent coverage and τ_d the average time for a diffusion jump, the exponent in Eq.(17) is independent of E_a [57].

At high temperatures the single adatom concentration is balanced by reevaporation (extreme incomplete condensation), thus $N(1) = R\tau_a$ is constant with $q = 2i^*/3$ and $E = 2(E_{i^*} + (i^*+1)E_a - E_d)/3$.

These arguments have been generalized by Stowell [47] to give an equation which describes analytically all three nucleation regimes, the "complete", "initially incomplete" as an intermediate case and "extreme incomplete" regime.

3. The steady–state regime is terminated by the onset of coalescence due to cluster growth. This regime is characterized by a sharp decrease of nucleation.

---

[2] The equivalent set of equations in the original literature [54] are differently grouped with

$$U_j = \rho_{in}(j)N(j)N(1) - \rho_{out}(j+1)N(j+1)$$

where U_j is a net rate at which single atoms form clusters with (j+1) atoms. Note that ρ_{in} ($cm^2 sec^{-1}$) and ρ_{out} (sec^{-1}) have different dimensions. But this notation emphasizes stronger the dependence of the single kinetic processes on monomer and cluster number densities.

Late Stage Cluster Growth. With the formation of first supercritical nuclei of the new phase cluster growth begins. The driving force is the Gibbs–Thomson effect (Eq.(5)) which favors larger clusters. During a first stage after the deposition stops the supersaturation is still high and the growth of the nuclei is a local effect with contributions from diffusing adatoms attaching to nearby clusters and coalescence when clusters are mobile. These processes decrease rapidly the supersaturation and the nucleation rate.

Late stage cluster growth starts when an average sized cluster is in microscopic balance with the adatom concentration. The first complete analytical treatment of the late stage growth regime was developed by Lifshitz and Slyozov [36, 37] and extended by Wagner [59]. Chakraverty [11] applied these concepts first to clusters on surfaces.

The description of the radial and time dependence of the cluster size distribution f(r,t) per unit area on the substrate, is based on three equations, (1) the Gibbs–Thomson effect, (2) mass transport equations and (3) the equation of continuity. Restricting the model to partial spherical clusters in their equilibrium shape[3] we note:

(1) The Gibbs–Thomson effect, (Eq.5), is written as a Taylor series expansion of the exponential term [59]:

$$c(r) = c_\infty \left(1+\frac{2\gamma_{av} v_M}{rkT}\right) \tag{18}$$

(2) The mass transport between clusters limits the rate of material flux. Two mechanisms are considered:

(i) For the surface diffusion mechanism the difference of the actual concentration at the cluster surface, c'(r), and the average free adatom concentration between the clusters, c_{free}, is the driving force for mass transport. Fick's second law of diffusion in cylindrical coordinates,

$$\frac{\partial c}{\partial t} = \frac{1}{r'}\frac{\partial}{\partial r'}(r' D_a \frac{\partial c}{\partial r'}) \, , \tag{19}$$

where r' and t are the radial and time parameter, has only a diverging logarithmic steady–state solution. The non–steady state solution to Eq.(19) is given by Crank [13] for a region bounded internally at r' = r sinΘ (see Fig. 2) with the concentration c_{free} for r' > r at t = 0 and c'(r) at r' = r for all times. The change in the amount of material by surface diffusion (Index D), dn_D/dt, is given by

$$\begin{aligned} \frac{dn_D}{dt} &= + 2\pi D_a r \sin\Theta \left(\frac{\partial c(r')}{\partial r'}\right)\Big|_{r'=r\sin\Theta} = \\ &= \frac{4D_a(c_{free}-c'(r))}{\pi^2 r\sin\Theta} \cdot \ldots \\ \ldots &\int_0^\infty du \frac{e^{-D_a u^2 t}}{u\left(J_o^2(r u \sin\Theta) + Y_o^2(r u \sin\Theta)\right)} \end{aligned} \tag{20}$$

where J_o and Y_o are zeroth order Bessel functions. Note that an analog equation was used in the discussion of the kinetic equations describing nucleation processes [54] (Eq.(13)). For short times, $\sqrt{D_a t} \ll r\sin\Theta$, Eq.(20) can be substituted by

$$\frac{dn_D}{dt} = -2\pi D_a (c'(r) - c_{free}) \left[\frac{2r\sin\Theta}{\sqrt{\pi}\Lambda} + \frac{1}{2} \pm \ldots\right] \tag{21}$$

Note that the diffusion length $\Lambda = 2\sqrt{D_a t}$ is time dependent and thus Eq.(21) is a non–steady state solution to the diffusion problem. We refer to this case as the "non–steady state diffusion" case. As pointed out by Chakraverty [11] a cluster growth mechanism with this equation governing the mass transport only works for a short time until diffusion gradients have built up. However, it might be a transient mechanism when a system crosses over from a growth mechanism without concentration gradients to the diffusion mechanism.

For long times, $\sqrt{D_a t} \gg r\sin\Theta$, a limit with a logarithmic correction term [45] replaces Eq.(21) [13]:

$$\frac{dn_D}{dt} = -4\pi D_a (c'(r) - c_{free}) \left[\frac{1}{\ln\left(\frac{4D_a t}{(r\sin\Theta)^2}\right)} - \ldots\right] \tag{22}$$

Chakraverty [11] proposed to introduce a "screening length factor" l_{sc} [39] to get a boundary condition at finite distance from the cluster: $c(r') = c_{free}$ for $r' = l_{sc} r\sin\Theta$. This assumption is crucial for the further calculations since otherwise a logarithmic dependence on time would additionally enter from the non–steady state solutions [45]. The screening length picture originates from concentration fluctuations superimposed on the concentration gradients due to randomly positioned neighbor clusters and therefore is not consistent with a mean field theory as developed in this section. With the second boundary condition c(r') = c'(r) for r' = rsinΘ and $l n l_{sc}$ in the range of 2 – 3 [63] the amount of material entering the cluster per unit time follows [13]

$$\begin{aligned} \frac{dn_D}{dt} &= 2\pi D_a r\sin\Theta \left(\frac{\partial c(r')}{\partial r'}\right)\Big|_{r'=r\sin\Theta} = \ldots \\ \ldots &= -\frac{2\pi D_a}{l n l_{sc}} (c'(r) - c_{free}) \end{aligned} \tag{23}$$

We refer to Eq.(23) as the "steady–state diffusion" case.

(ii) For an interface transfer mechanism due to an energy barrier at the cluster surface the origin of the mass transport is the difference between the equilibrium concentration at the cluster surface (Gibbs–Thomson equation, Eq.(18)), c(r), and the actual concentration at the surface, c'(r). The change in the amount of material by interface transfer (index T), dn_T/dt, is expressed using a rate constant κ [59]

$$\frac{dn_T}{dt} = -S_T \kappa (c(r) - c'(r)) \tag{24}$$

The term S_T represents the cluster surface involved in the mass transfer. We distinguish two cases for S_T: the interface transfer passes either the full cluster surface with $S_T = 4\pi r^2 \alpha_2(\Theta)$ [11][4] or only the contact line of the cluster at the substrate surface with $S_T = 2\pi r \alpha_3(\Theta)$ [63], assuming a lower

[3] Other cluster shapes, e.g. two–dimensional islands [63] or crystalline clusters [59] can be treated similarly.

energy barrier for atoms at this specific cluster site. Note that κ corresponds to a probability factor (dimension sec^{-1}) in the first case which we designate as κ_a with index a for areal, and to a speed constant for mass transfer (dimension cm/sec) in the latter case designated as κ_r with index r for radial.

The equations for mass transport by surface diffusion (Eq.(23)) and interface transfer (Eq.(24)) are combined to eliminate the concentration c'(r). For a steady–state mass transfer both rates must be equal [59], yielding

$$\frac{dn}{dt} = -\frac{2\pi S_T\,(D_a\kappa/l n l_{sc})}{(2\pi D_a/l n l_{sc}) + S_T\kappa}\,(c(r) - c_{free}) \qquad (25)$$

Eq.(25) for the mass transport and the Gibbs–Thomson equation (Eq.(18)) combine to a complete description of the change of cluster radius with time. Small clusters decompose since their equilibrium concentration exceeds the free concentration and clusters with large radii grow (Ostwald ripening). Of special importance is the radius of the clusters in equilibrium with the free concentration, which we define as the "critical radius" r_c:

$$c(r_c) = c_{free} \qquad (26)$$

Note that r_c is a function of time in the case of ripening. It may not be mixed up with the critical radius r_k as defined for nucleation studies above. Based on Eq.(26) and the Gibbs–Thomson equation, Eq.(25) is rewritten for the change of radius with time:

$$\frac{dr}{dt} = 4\pi\frac{\alpha_2(\Theta)}{\alpha_1(\Theta)}\frac{\gamma_{av}v_M^2 c_\infty}{kT}\frac{S_T D_a\kappa}{S_C(2\pi D_a + S_T\kappa l n l_{sc})}\left(\frac{1}{r_c} - \frac{1}{r}\right) \qquad (27)$$

From Eq.(27) all specific cases are derived in the universal form

$$\frac{dr}{dt} = -\frac{\beta}{r^n}\left(\frac{1}{r} - \frac{1}{r_c}\right) \qquad (28)$$

with n depending on the dimensionality of the system and the process limiting the mass transport:

1. n = 0. This value corresponds to two–dimensional islands ($S_T = S_C = 2\pi r$) with the interface transfer limiting the mass transport: $D_a > r\kappa_r l n l_{sc}$ [63]. Alternatively it applies to three–dimensional clusters with the full cluster surface active in the mass transport ($S_T = S_C = 4\pi\alpha_2(\Theta)r^2$) and the interface transfer limit given by $D_a > 2\alpha_2(\Theta)r^2\kappa_a l n l_{sc}$ [11]. β is given by $\beta = (2\alpha_2(\Theta)\gamma_{av}v_M^2 c_\infty\kappa_a)\ /\ (\alpha_1(\Theta)kT)$.

2. n = 1. This value is given for two–dimensional islands with the surface diffusion limiting the mass transport $D_a < r\kappa_r l n l_{sc}$. β is given by $\beta = (2\gamma_{av}v_M^2 c_\infty D_a)\ /\ (kT l n(l_{sc}))$. All cases discussed so far yield the same exponent n for Eq.(28) as found for three–dimensional clusters in a bulk solution [37, 59]. We refer to these cases therefore as "quasi bulk cases".
   The same value for n is realized for three–dimensional clusters with the contact line to the substrate active in the mass transport which is limited by the interface transfer mechanism, $D_a > r\kappa_r l n l_{sc}$ [63]. β is given by $\beta = (\alpha_3(\Theta)\gamma_{av}v_M^2 c_\infty\kappa_r)\ /\ (\alpha_1(\Theta)kT)$.

3. n = 2. This value is obtained for three–dimensional clusters with the mass transfer limited by surface diffusion, $D_a < r\kappa_r l n l_{sc}$ or $D_a < 2\alpha_2(\Theta)r^2\kappa_a l n l_{sc}$ [11]. β is given by $\beta = (2\alpha_2(\Theta)\gamma_{av}v_M^2 c_\infty D_a)\ /\ (\alpha_1(\Theta)kT l n(l_{sc}))$. Since the last two cases contain an additional $\frac{1}{r}$ term as compared to the corresponding bulk cases, we refer to them as "true surface cases".

(3) An analytical treatment of ripening requires equations connecting the cluster size distribution with above growth rates of the cluster radii. The cluster size distribution is introduced by two conservation laws, the conservation of mass and the conservation of larger clusters, connected to the equation of continuity: since we exclude coalescence, the total number of clusters is only altered by formation and dissociation of the smallest clusters in the vicinity of r = 0. For all larger radii the total number of clusters is conserved [14, 37]:

$$\frac{\partial f(r,t)}{\partial t} = -\frac{\partial}{\partial r}\left(f(r,t)\,\frac{dr}{dt}\right) \qquad (29)$$

For an explicit solution of Eq.(29) $\frac{dr}{dt}$ is used from Eq.(28) yielding an equation of motion for the cluster size distribution f(r,t). The time dependence of the critical radius follows by analytical calculation:

$$r_c(t) = r_c(0)\left(1 + \frac{t}{\tau_c}\right)^{\frac{1}{n+2}} \qquad (30)$$

with

$$\tau_c = \left(\frac{3}{n+2}\right)\frac{\nu_n r_c^{n+2}(0)}{\beta} \qquad (31)$$

Considering the different n values in connection with Eq.(28) we note: the differences in the time dependence of the critical radius arise from the different r dependences in the mass transport equations Eq.(23) and Eq.(24) and an additional $\frac{1}{r}$ term for the ratio of the active surface for the mass transport to the total surface of the clusters, i.e. S_T/S_C, for true surface systems (Eq.(27)).

Two–dimensional islands grow with $r_c \propto t^{1/2}$ in the interface transfer limit and with $r_c \propto t^{1/3}$ in the surface diffusion limit. Three–dimensional clusters grow with $r_c \propto t^{1/2}$ or $r_c \propto t^{1/3}$ in the interface transfer limit depending on the fraction of the cluster surface involved in the mass transport and grow with $r_c \propto t^{1/4}$ in the surface diffusion limit.

Experimental Results and Discussion

Ion Scattering Experiments. The experimental tech-

[4] $\alpha_1 - \alpha_3$ are geometrical factors for partial spherical clusters. They are defined by the volume of a cluster $V_C = \frac{4}{3}\pi\ r^3\alpha_1(\Theta)$ with $\alpha_1(\Theta) = \frac{1}{4}\ (2 - 3\cos\Theta + \cos^3\Theta)$, the surface of the cluster $S_C = 4\pi r^2\alpha_2(\Theta)$ with $\alpha_2(\Theta) = \frac{1}{2}\ (1 - \cos\Theta)$ and the periphery line of the cluster, $2\pi r\alpha_3(\Theta)$ with $\alpha_3(\Theta) = \sin\Theta$ [11].

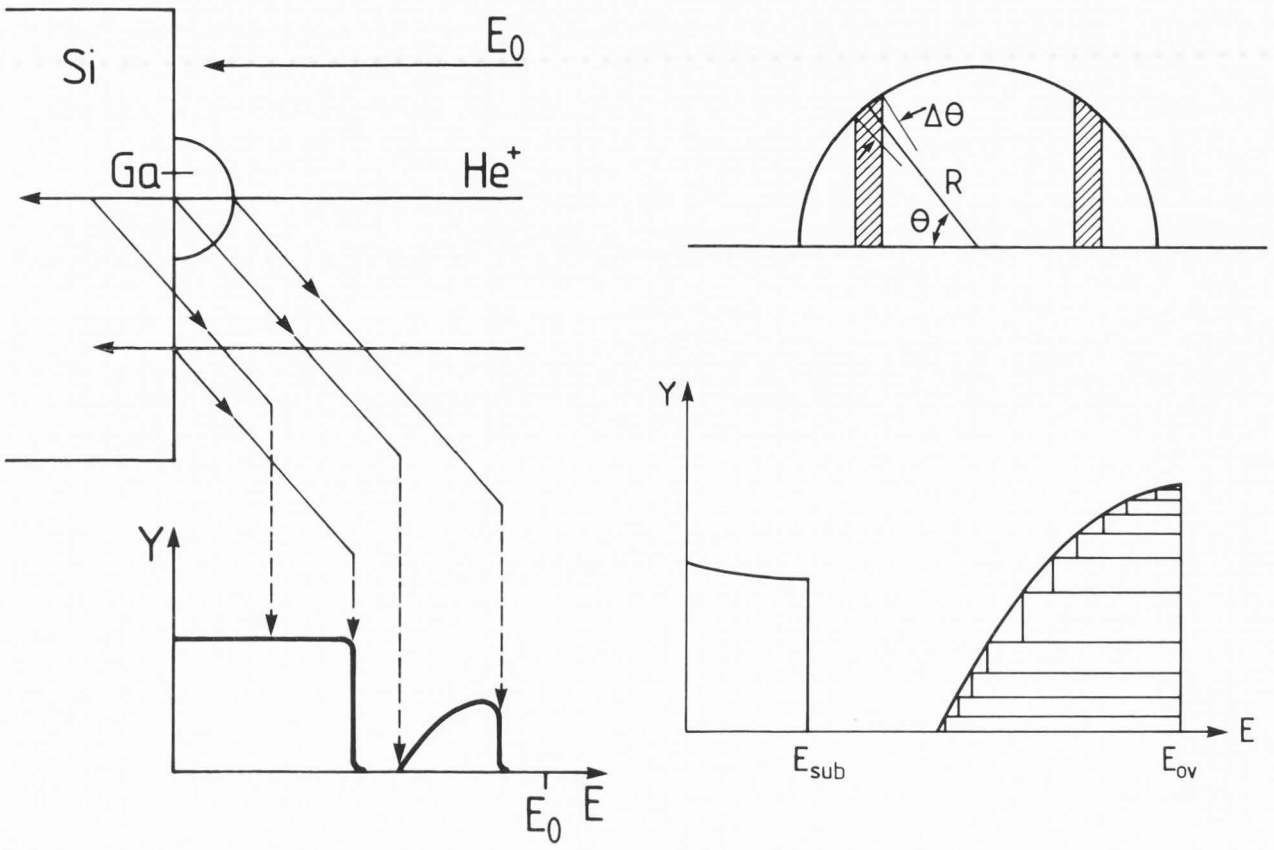

Fig.4. Schematics of the energy distribution and the scattering process in standard Rutherford backscattering for hemispherical clusters on a surface. left: scattering process; right: calculated spectrum of a hemispherical cluster.

nique to analyse clustered systems by Rutherford backscattering techniques (RBS) is first described. In the discussion data on Sn cluster growth on differently prepared Si surfaces serve as an illustration of the interpretation of cluster growth measurements based on the above model.

Samples were prepared in an ultra–high vacuum system (base pressure $< 5 \times 10^{-9}$ Pa) [70, 71] containing Si, Sn and Ga sources and equipped with standard surface analytical tools including a Van de Graaff accelerator for ion scattering analysis [16, 17]. Measurements were carried out on (a) Si(111) and Si(100) surfaces to explore the effect of surface structure, and (b) on surfaces prepared by (1) in–situ sputtering and annealing to 1200 K, (2) chemical etch prior to insertion into the vacuum system and annealing at 1070 K [30], and (3) Si–buffer layer deposition to explore the effects of surface preparation in the clustering process. Samples were heated radiatively; the temperature was determined from the heating current which had been previously calibrated using a thermocouple attached to the sample and which had been controlled by an infrared thermometer.

Clean surfaces, as indicated by Auger spectroscopy, displayed sharp 7x7 for Si(111) and 2x1 low–energy electron diffraction (LEED) pattern for Si(100). Metal deposition was

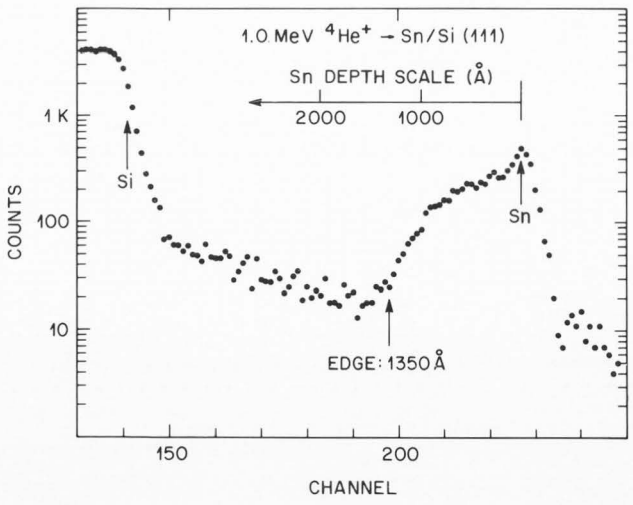

Fig.5. Ion scattering spectrum for Si(111)7x7 after deposition of about 6 ML equivalent coverage of Sn and annealing at 300°C. The Sn and Si edges are indicated. A depth scale for scattering in Sn is given at the top.

carried out at rates of $\sim 1 \times 10^{14}$ $cm^{-2}sec^{-1}$, Si–buffer layers were deposited at $\sim 1 \times 10^{15}$ $cm^{-2}sec^{-1}$ with the sample at 600°C. Si–buffer layer thicknesses were measured by RBS from a graphite single–crystal backing mounted close to the Si sample.

The spectrum of a clustered structure using hydrogen or helium ion beams with energies typically 0.5 to 2 MeV and a backscattering geometry is illustrated in Fig. 4 [18]. Ions in a beam of larger diameter than the cluster are backscattered from atoms of the cluster at any depth between the cluster surface and the substrate interface with a yield proportional to the cluster material at the respective depth. If the mass of the substrate atoms is smaller than the mass of cluster atoms, the substrate contribution to the energy spectrum is shifted to lower energies due to the kinematic of the scattering process [16].

Experimentally observed spectra result if the ideal spectrum (Fig. 4) is further convoluted by two additional contributions: the real cluster size distribution and the experimental depth resolution. As long as the cluster size distribution is not too broad the height of an average sized cluster, h_C, can be extracted from the ion scattering spectrum.

The experimental depth resolution of the detection system in RBS limits the observation to cluster heights larger than 10 nm. This limit is due to the $\sim$ 10 keV energy resolution of solid state particle detectors. It can be improved by replacing the solid state detector with an electrostatic analyzer detection system with typical energy resolution of $\Delta E/E = 4 \times 10^{-3}$ [53]. Using H^+ beams of 50 – 100 keV or He^+ beams of 100 – 200 keV (medium energy ion scattering "MEIS") this corresponds to a depth resolution of 0.5 – 1 nm [16, 53].

Fig. 5 shows a spectrum obtained with 1.0 MeV He^+ ions on a Si(111) sample covered with Sn clusters [70]. A maximum cluster height can be extracted in the accessible range of heights from $\sim$ 20 nm to $\sim$ 300 nm. If the cluster shape is known, e.g. from microscopic measurements, an improved resolution and a lower limit of height detection are achieved by tilting the sample relative to the incident beam.

If the mass of the cluster atoms is smaller or equal to the mass of the substrate atoms, e.g. Ga clusters on a GaAs substrate, standard RBS spectra do not reveal clustering due to relative count rate statistics of substrate and clusters. However, cluster height measurements are still possible aligning the incident ion beam with a channel direction of the substrate lattice reducing the substrate related count rates by one to two order of magnitude [16]. This is shown in Fig. 6 for 1.8 MeV He^+ incident on a Ga covered GaAs(100) sample. In such measurements the accuracy of the obtained cluster heights is slightly reduced.

Cluster analysis solely based on depth profiling techniques as ion scattering is not possible, since several different processes on surfaces can yield qualitatively identical spectra. Such effects are

1. bulk in– or interdiffusion of film atoms and substrate atoms,

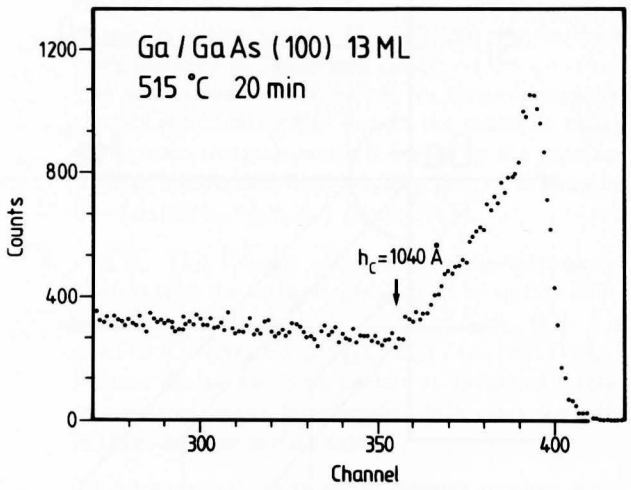

Fig.6. RBS measurement of Ga cluster growth on GaAs(100). Samples were ex–situ chemically oxidized and in–situ annealed to 600°C to obtain a c(2x8) LEED pattern. 13 ML equivalent coverage of Ga measured in normal incidence channeling condition after post–deposit anneal for 20 min to 515°C. The average cluster height, h_C, is 104 nm.

2. reactive compound formation (e.g. metal silicide formation),

3. substrate material segregation penetrating the film bulk material or along grain boundaries and

4. cluster formation.

Note that the same restrictions apply to attenuation based techniques as Auger electron intensity measurements as a function of coverage. To discriminate these processes additional techniques are required, e.g. electron microscopic techniques to direct imaging clusters (see below).

Nucleation Experiments. The first data on nucleation were obtained by electron microscopy for metals on alkali halides [44]. Nucleation rates, J, are measured as a function of the deposition flux yielding critical cluster sizes, i*, from Eq.(9). E.g. for Au/KCl Stowell [47] showed that $J \propto R^2$ corresponding to $i^* = 1$ [57].

From measurements of the maximum cluster density, N_x, as a function of temperature activation energies E_a (at higher temperatures), E_d and E_{i^*} are obtained based on Eq.(17). An example of such an analysis is illustrated based on data by Hanbücken, Futamoto and Venables [28, 55] for the system Ag/Si(100) (Fig. 7).

Activation energies are deduced using the equation of the maximum cluster density for the complete condensation regime (when reevaporation is excluded) [55, 56]. These energies are obtained based on a two–dimensional nearest neighbor pair bond model on a hexagonal lattice with the pair binding energy E_b and the activation energy of surface diffusion E_d as free parameters. The additional numbers indicated per line

segment in Fig. 7 correspond to the number of atoms in the critical cluster, i^*, for each temperature regime as obtained from a separate model calculation [56]. This calculation yields all critical nuclei sizes possible based on the criterion of minimum nucleation density. The values of i^* are defined if an additional atom forms three new bonds to the island periphery. Corresponding numbers of bonds per critical island are obtained and used in the data analysis to determine E_{i^*}, $E_{i^*} = b_{i^*} E_b$. The different factors $b_{i^*}/(i^* + 2)$ and $i^*/(i^* + 2)$ for the two free parameters in each temperature segment allow one to separate both activation energies in a single Arrhenius-type measurement as shown in Fig. 7.

Note the specific assumptions considered for Ag on Si surfaces [55]:

1. critical clusters are two-dimensional islands with a hexagonal bond structure; thus all b_{i^*} are known,
2. the energetic difference of silver in islands and silver monomers is described by a nearest neighbor pair bond model neglecting altering contributions from the substrate as expected for covalent binding adlayers or three-dimensional critical clusters and
3. defect induced, i.e. heterogenous, nucleation and island mobility are excluded.

Activation energies obtained for Ag on Si are included in Table 2 for comparision with results from cluster growth studies.

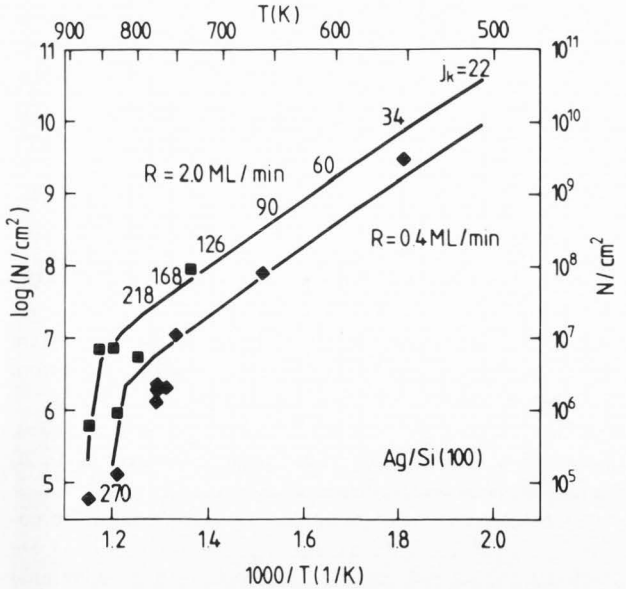

Fig.7. Measurement and calculation of the maximum stable cluster density for Ag/Si(100) with $E_b = 0.1$ eV, $E_d = 0.7$ eV and $E_a = 2.6$ eV. The upper line represents data with R = 2.0 ML/min (□) and the lower line represents data with R = 0.4 ML/min (◇). Reprinted with permission from Ref. [28].

Discussion: The system Sn on Si. Figs. 8 and 9 show cluster height measurements for different coverages of Sn on Si(111) and Si(100). After deposition at room temperature the samples were held at the indicated temperatures with the cluster height repeatedly measured. The fourth power of the cluster height, h_C, versus time is plotted as the proper linearization for the ripening case with surface diffusion limiting the mass transport. A linear fit is in excellent agreement with the data at later times for both, Si(111) and Si(100) substrates, but clearly deviates at shorter times. This early part can be fit satisfactorily with a cubic power of the cluster height proportional to time. The rates for the early growth, $\Delta h^3/\Delta t$, are the same in both cases of Fig. 9. The growth rates $\Delta h^4/\Delta t$ differ at most by 15% for the late regime despite a drastic difference in the starting coverage of a factor 6. (If a correction is made for the non-clustering Stranski-Krastanov layer thickness of 1.7 monolayer equivalent coverage of Sn, the starting coverages differ by a factor of 10).

We now consider two reasons for the late transition to the $t^{1/4}$ dependence: (1) The interface transfer limit may dominate at short times. Following Wynblatt and Gjostein [63] we test the condition for the diffusion limit $\kappa_r \ln(l_{sc}) \gg D_a$ for Eq.(27). The diffusion coefficient can be written as:

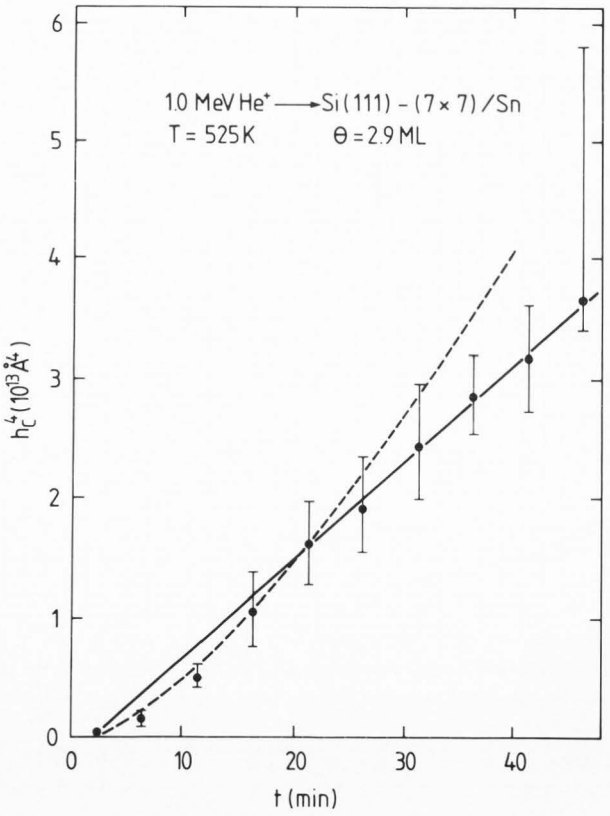

Fig.8. RBS measurement of the fourth power of the cluster height as a function of time for 2.9 ML equivalent coverage of Sn on Si(111) deposited at room temperature and held at 525 K.

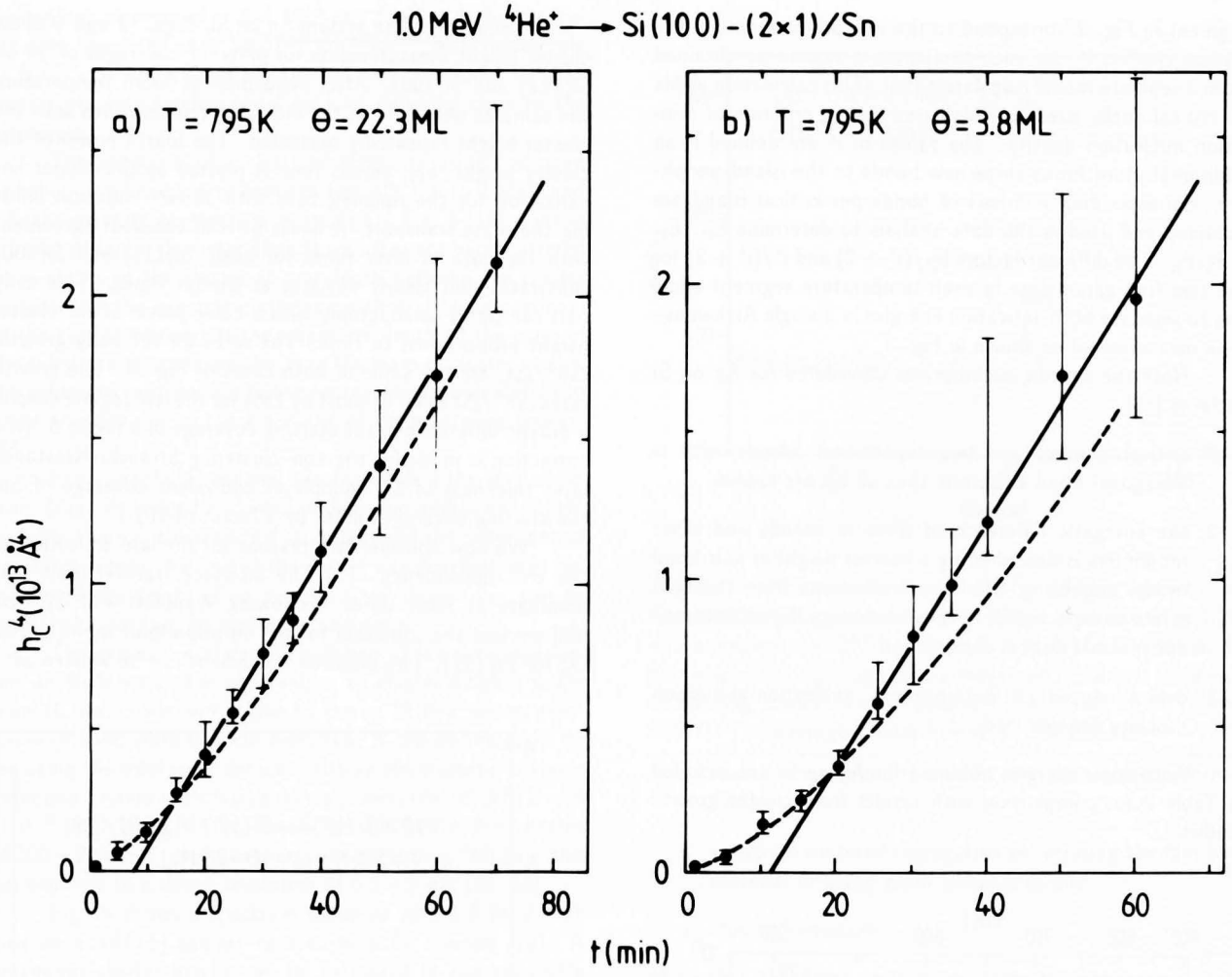

Fig.9. Power law dependence of the height of clusters as a function of time at 795 K for two different coverages on Si(100)2x1. (a) 22.3 ML equivalent coverage of Sn and (b) 3.8 ML equivalent coverage of Sn. The solid line corresponds to the fourth power dependence of the cluster height and the dashed line to the cube of the cluster height.

$$D_a = a^2 \nu_s \exp\left(\frac{S_m^s}{k}\right) \exp\left(-\frac{E_d}{kT}\right) \qquad (32)$$

where the jump distance is approximated by the lattice constant of the substrate, a, ν_s is the vibration frequency of an adatom, S_m^s is the entropy of migration. κ_r is given by [63]:

$$\kappa_r = a\nu_{as} \exp\left(-\frac{E_d}{kT}\right) \qquad (33)$$

Thus surface diffusion dominates if: $a \exp(S_m^s/k) \gg r \ln(l_{sc})$. With [63] $1 < \exp(S_m^s/k) < 10$ the cross over in the mass transport limit occurs already for very small clusters.

(2) For early times deviations may origin from the introduction of the screening length factor. The assumption that the diffusion gradients have built up requires that the diffusion length, Λ with $\Lambda = \sqrt{D_a t}$, reaches beyond next neighbour clusters. We estimate the significance of this assumption by comparing the cluster spacing and the diffusion length at the time of the transition for Sn on Si(111): the cluster spacing after 20 minutes is roughly 3 μm (from scanning electron microscopy measurements). Using the Einstein relation, with the surface diffusion coefficient estimated from the activation energy of clustering, $D_a(525\ K) = 3 \times 10^{-11}$ cm^2/sec [68], we get a diffusion length of 3.5 μm. Thus, the steady–state diffusion model applies only after 15 to 20 minutes in the reported experiments.

Finally we compare the proposed ripening model to coalescence growth. Since all experiments in this section are done under mass conservation conditions, i.e. no additional material is deposited during cluster growth, coalescence events would require motion of entire clusters, e.g. by Brownian motion. As discussed by Dunning [14] this process also results in a power law dependence of the cluster radius as a function of time. However, the time constant in Eqs.(30) and (31) depends inversely on the starting coverage, i.e. the to-

tal amount of clustering material, as opposed to the Ostwald ripening model. Fig. 9 shows a comparision of growth rate measurements for two different starting coverages of Sn on Si(100) at the same temperature. The late stage growth rate differs only at maximum by 15%. Therefore the experimental result of Fig. 9 strongly supports the assumption that coalescence can be excluded in these experiments.

Note that temperature dependent growth rate measurements based on Eq.(30) do not correspond to a simple activation process and an Arrhenius plot should give an non–linear graph due to the additional T term in β from the Gibbs–Thomson equation. This is tested in Fig. 10 for Ga on Si(100) and Si(111). The narrow temperature range of the measurements leads only to a small deviation from the equivalent behaviour of a simple activation process with activation energy E_c. In Table 2 for a wide range of systems the measured activation energies are summarized and compared to diffusion data determined by other techniques. Note that E_c is the sum of all activation energies occuring in the cluster growth process. In addition to the activation energy of surface diffusion the enthalpy of formation of a cluster from single atoms enters as shown by the following argument [65].

Assume a system with the cluster phase already formed. The chemical potentials of both phases, the adatom phase (index free) and the cluster phase (index C), are equal in equilibrium [38]

$$\mu_C(c_C, T) = \mu_{free}(c_{free}, T) \qquad (34)$$

The dependence on the number of atoms in a cluster, c_C, can be neglected [38]. Is the free adatom phase dilute, i.e. $c_{free} \ll 1$, then the chemical potential per adatom is given by [40]

$$\mu_{free}(c_{free}, T) = \mu^o_{free}(T) + kT \ln(c_{free}(T)) \qquad (35)$$

where $\mu^o_{free}(T)$ is the standard chemical potential for a full monolayer equivalent coverage. Inserting Eq.(35) in Eq.(34) results in:

$$\ln(c_{free}(T)) = \frac{1}{kT}(\mu_C(T) - \mu^o_{free}(T)) \qquad (36)$$

The difference on the right hand side equals the difference in enthalpy for the formation of free adatoms from atoms in a cluster, E_f, when E_f is not a function of temperature:

$$\ln(c_{free}(T)) = -\frac{E_f}{kT} + const \qquad (37)$$

Note the equivalence to the three dimensional integrated Clausius–Clapeyron equation for vaporization of an ideal gas [38].

Thus the activation energy of clustering, determined from an Arrhenius type of data analysis based on Eq.(30) is the sum of E_d and E_f. An equivalent argument was given by Wynblatt and Gjostein [63] based on an atomic picture[5].

Absolute values of c_∞ can be determined based on

[5]Note that the ratio of E_f and E_b depends on the geometrical cluster model. E.g. for two–dimensional Ag islands forming on Si(111) [28] we find $3E_b = E_f$.

Table 2: Activation energies for clustering, E_c, from nucleation and cluster growth experiments.

System	E_c (eV)	Method
Sn/Si(111)	0.32 ± 0.04	RBS/SEM
Sn/Si(100)	1.0 ± 0.2	RBS/SEM
Ge/Si(100)	1.0 ± 0.1	RBS/SEM/TEM
Ga/Si(111)	0.49 ± 0.05	RBS/REM
Ga/Si(100)	0.80 ± 0.07	RBS/REM
Ga/Si(100) 4^o miscut	0.80 ± 0.07	RBS/REM
Ga/As/Si(111)	1.23 ± 0.05	RBS/REM
Ga/GaAs(100)	1.15 ± 0.20	RBS/REM/SEM
Ag/Si(100) [28, 55]	1.0	SEM
Ag/Si(111) [28]	0.65	SEM
GaAs/Si(100) [7]	0.7 ± 0.4	TEM/SEM
GaAs/Si(100) [6]	1.0 ± 0.1	TEM
Ga/GaAs(100) [41]	1.3 ± 0.1	RHEED
Sn/GaAs(100) [29]	1.8 ± 0.3	TEM

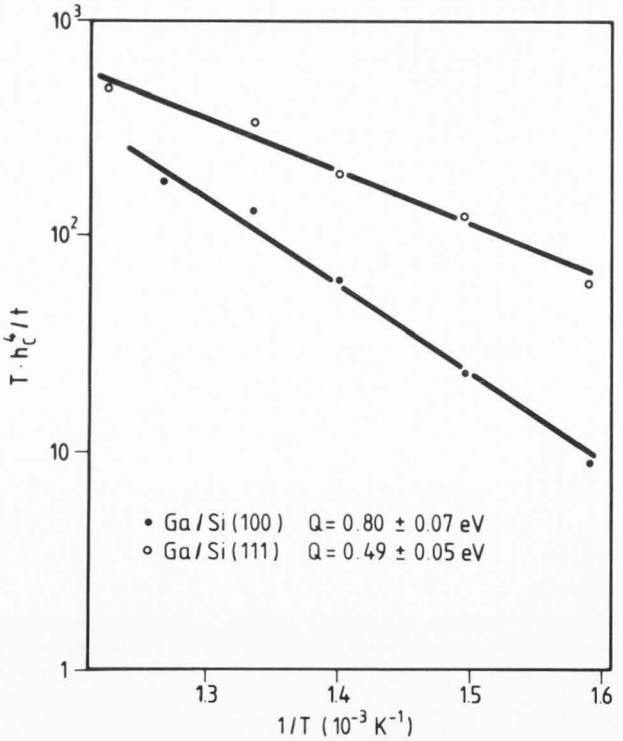

Fig.10. Arrhenius plot of growth rates of Ga clusters on Si(100) and Si(111) to obtain activation energies for the clustering process. The additional temperature factor on the ordinate is due to the ripening model involving the Gibbs–Thomson equation.

Eq.(36) [65] with chemical potentials deduced from molecular dynamics simulations [26]. Still determining preexponential factors for the clustering process requires to estimate all constants in Eq.(30) leading to large error margins.

We now want to discuss how the activation energies of clustering determined from the late stage cluster growth are related to surface diffusion coefficients. From Fig. 1 follows that an atom in a cluster of a Stranski–Krastanov system is energetically in a similar configuration as an atom on the surface between the clusters, i.e. E_f is small. From above discussion and the data measured by Venables et al. [28] we estimate 0.05 eV/atom $\leq E_f \leq$ 0.3 eV/atom with the lower limit representing the difference in energy for an atom in an additional coherently strained full layer [15]. Thus the activation energy of clustering is governed by the activation energy of diffusion. For Volmer–Weber systems this argument fails and E_f can be a rather large value. Therefore experimental activation energies of clustering are expected higher than those for Stranski–Krastanov systems.

Further evidence supporting the interpretation of the data based on surface diffusion arises from microscopic measurements. For Ga on Si(111) and Si(100) we found the same shape of clusters by reflection electron microscopy (REM, Fig. 11) [66]. This observation implies that the surface tensions, which define the contact angle of clusters on a surface, do not alter from one Si face to the other. Still, the activation energy for clustering differ strongly (see Table 2). Since the activation energy for clustering is very different yet the cluster shape (Ga–Ga interaction) is the same we conclude that surface diffusion is the origin of the different activation energies of clustering.

A similar argument results from Fig. 12 comparing the growth rates of Sn clusters on Si(111) substrates for different surface preparations at 570 K. The large dependence on growth rate is inconsistent with a mass transport dominated by a cluster formation energy but is easily explained by differences in surface structure and roughness influencing the diffusion barrier heights.

Surface Diffusion Coefficients: Concentration Dependence

The surface diffusion coefficient D_a used in Eq.(27) is not identical to the surface diffusion coefficient deduced from mass transport experiments with micrometer resolution [9, 10, 49] as shown by the following argument [12, 21, 23, 64]. In a random–walk model of a clustered system an adatom spends a fraction of time in nearby clusters (Fig. 13). Both, adatom state (1) and cluster sites (2) have to be considered and an average jump frequency $(1/\tau)$ rather than a specific jump frequency for the adatom is required for the basic Einstein relation,

$$D_s = \frac{a^2}{2}\frac{1}{\tau}\,, \tag{38}$$

approximating the jump distance by the lattice constant. D_s is the "mass transfer" or "chemical" diffusion coefficient while the diffusion coefficient in Eq.(27) is the "intrinsic" diffusion coefficient [24]. D_s corresponds to diffusion on terraces in the presence of clusters, i.e. with the moving species sticking to the clusters for some time, and D_a corresponds to the adatom diffusion on a terrace. The mean jump frequency $(1/\tau)$ is the sum of the site specific jump frequencies, $(1/\tau_i)$, times the probability P_i to populate this site,

$$\frac{1}{\tau} = \sum_i \left(\frac{1}{\tau_i} P_i\right) = \sum_i \left(\frac{c_i/c}{\tau_i}\right) \tag{39}$$

The probability term in Eq.(39) is replaced by the ratio of adsorbed atoms in specific sites to the total number of adsorbed atoms. If we consider only the adatom state (index a) to contribute to the mass transport over the surface (neglecting e.g. sites on steps), we get [64]

$$D_s = \frac{a^2}{2}\frac{c_{free}}{c}\frac{1}{\tau_{free}} = D_a\frac{c_{free}}{c} \tag{40}$$

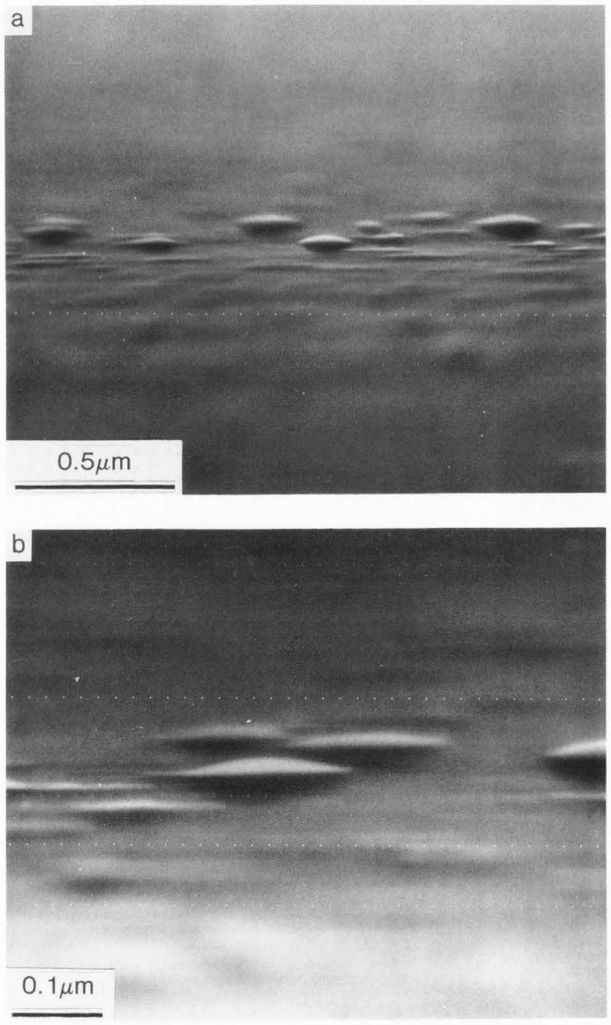

Fig.11. Reflection electron microscopy pictures of Ga clusters on (a) Si(111), grown at 750 K for 100 min and (b) Si(100), grown at 715 K for 60 min.

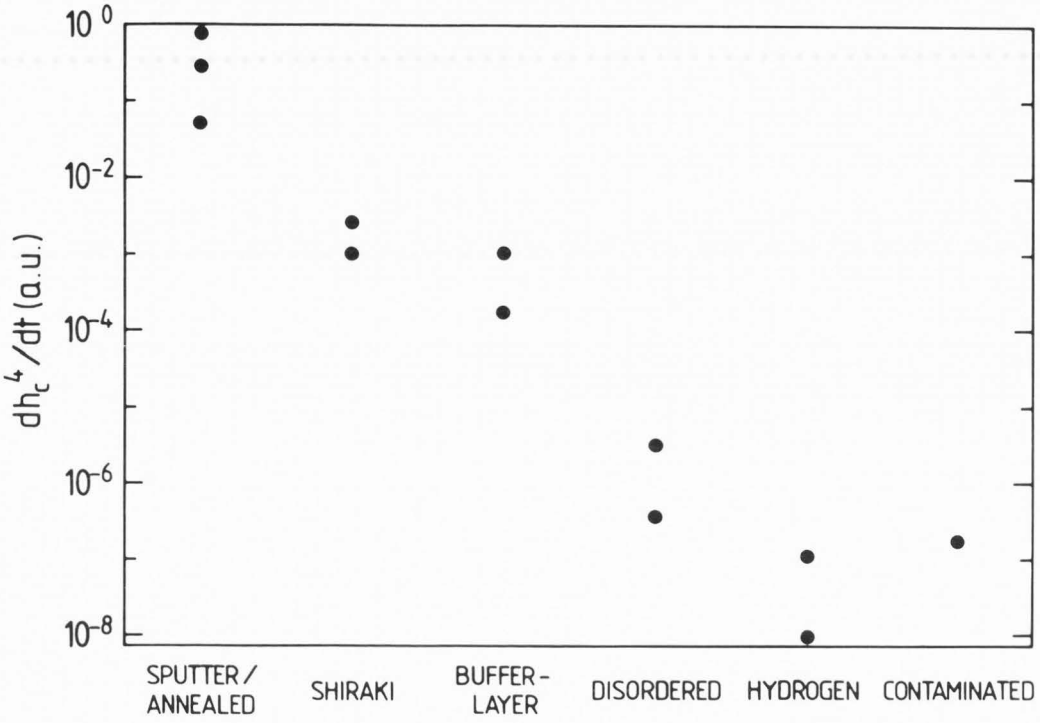

Fig.12. Affinity for clustering for different treatments of a Si(111) substrate surface before deposition of Sn and annealing at 570 K. For the "Shiraki" cleaning method (ex–situ chemical oxidation and in–situ low temperature oxide desorption) see Ref. [30].

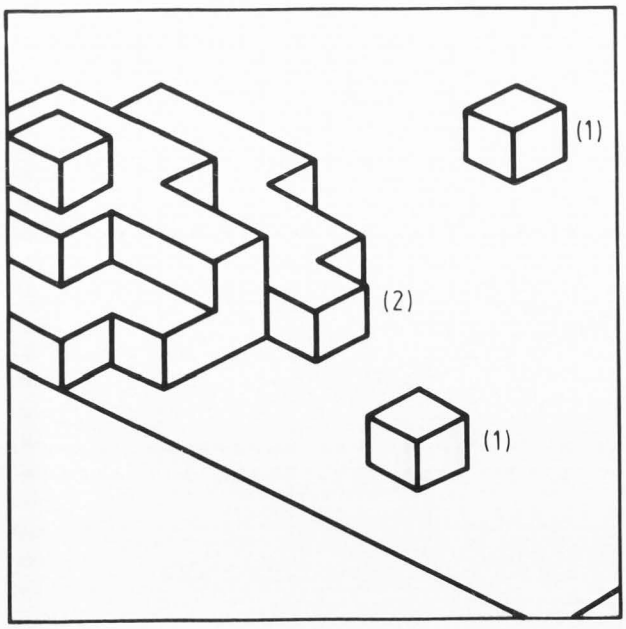

Fig.13. Sketch showing the different sites discussed for hetero–surface diffusion in a clustering system.

Eq.(40) shows that we have to distinguish between the two diffusion coefficients in order to discuss the concentration dependence of surface diffusion in clustered systems. Since all constants in Eqs.(27) and (28), including dr_c^{n+2}/dt and c_{free}, the adatom concentration, do not depend on coverage ($c_{free} = c_\infty$ approximately for large clusters) we find that $D_a \neq f(c)$. This result is not surprising in the clustered regime, since despite changes in the total coverage the local adatom concentration on the terrace does not change. The concentration dependence of D_s follows form Eq.(40) [64]

$$D_s \propto \frac{1}{c} \tag{41}$$

or

$$D_s \propto \frac{1}{c - c_t} \tag{42}$$

The term c_t in Eq.(42) represents a constant fraction of the adsorbed species which does not contribute to the clustering process in the Gibbs–Thomson equation, but contributes only to the uniform layer thickness between clusters as observed in experiments. We expect $c_t \neq 0$ for systems growing in the Stranski–Krastanov growth mode [2, 3] and $c_t = 0$ for systems growing in the Volmer–Weber growth mode. Note that these results do not depend on the dimension of the clusters, i.e. whether two–dimensional islands or three–dimensional clusters form.

We compare this result with literature data for systems obtained by microscopic mass transport techniques which measure D_s.

Ag/Ge(111). Suliga and Henzler [49] measured surface diffusion for semi–infinite steps of Ag on Ge(111) by scanning Auger microscopy. The details of this technique are discussed in another paper in this volume [25]. Concentration profiles yielding concentration–dependent surface diffusion coefficients were analyzed with the Boltzmann–Matano data analysis technique [13]. The authors interpreted the observed concentration dependence qualitatively with a defect formation model. Fig. 14 shows the data taken from three different samples miscut by 0° to 6°. The original data are shown in the inset; the main plot displays linearly renormalized diffusion coefficients in order to eliminate the step density dependence. The dashed line is a fit based on relation (41) and the solid line is a fit based on relation (42) with $c_t = 0.18$ ML. Due to the experimental uncertainty of the measured coverages we have to consider $0.15 \leq c_t \leq 0.23$ ML overlapping with the 4x2 ordered structure observed by low–energy diffraction (LEED).

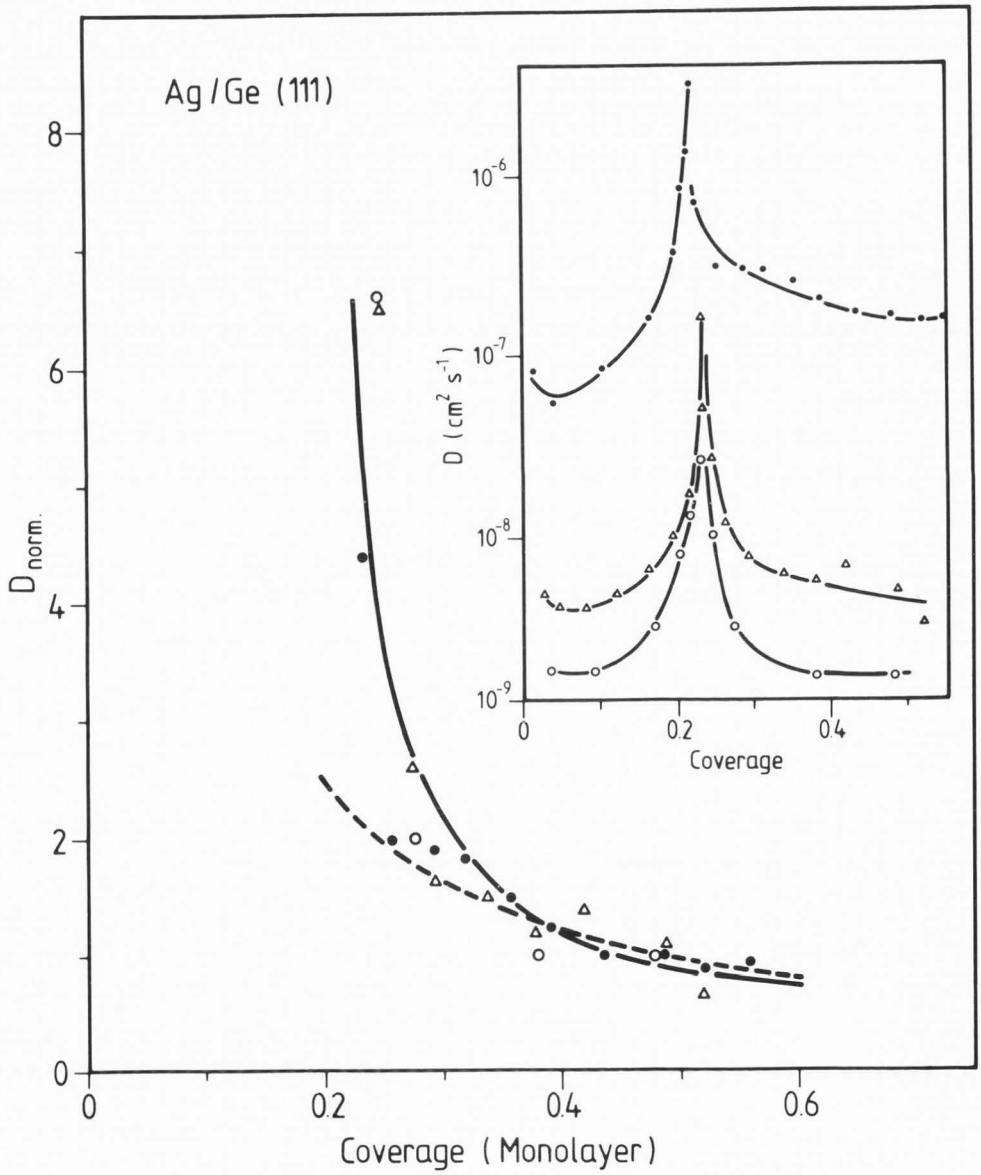

Fig.14. Normalized diffusion coefficients for Ag/Ge(111) at 450°C for different miscut samples: 0.0° ± 0.07° (○), 0.9° ± 0.07° (△) and 5.9° ± 0.3° (●). The solid line is based on Eq.(42) with $c_t = 0.18$ ML, the dashed line is based on Eq.(41). The inset shows the original data from Ref. [49].

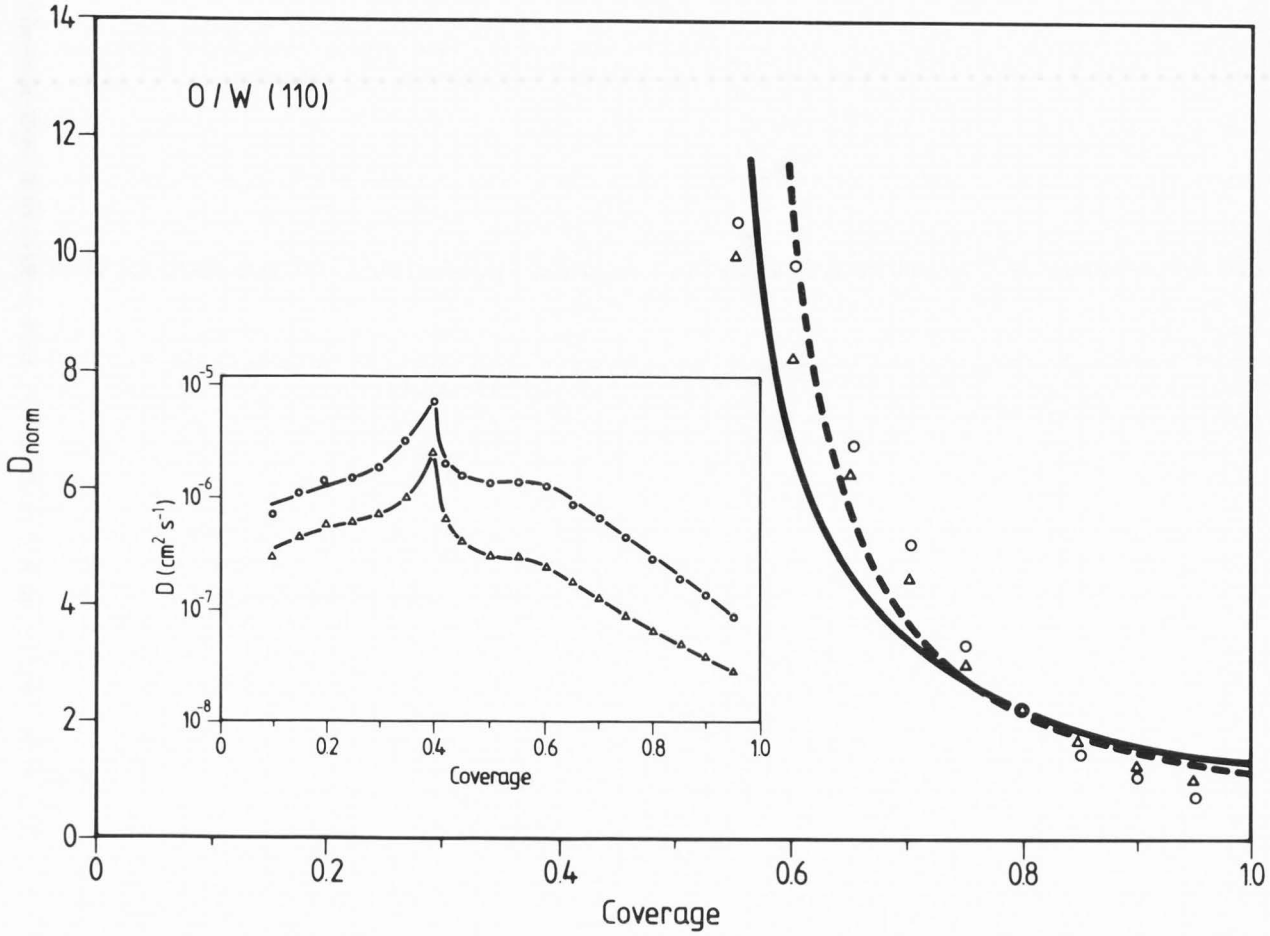

Fig.15. Normalized diffusion coefficients for O/W(110) at 880°C (○) and 760°C (△). The solid line is based on Eq.(42) with c_t = 0.5 ML and the dashed line with c_t = 0.55 ML. The inset shows the original data from Ref. [9].

O/W(110). After preparation of semi–infinite steps of oxygen on W(110), Butz and Wagner [9] used a capacitor geometry to measure the surface diffusion profiles. The capacitor was formed by a 6 μm tungsten wire as the vibrating reference electrode and the sample as the counter electrode. The lateral varying oxygen coverage was measured by the variation of the surface potential as recorded by contact potential differences. Fig. 15 displays the original data (see inset) eliminating the temperature dependence of two sets of measurements. Agreement with the data is reached using relation (42) with c_t roughly at 0.5 ML. This is in accordance with the finding that oxygen forms two–dimensional islands which merge as the concentration approaches 0.5 ML. Below a half–monolayer, diffusion of single adatoms does not occur, rather domain boundary growth is observed [52]. A drastic change in the sticking coefficient upon deposition beyond 0.5 ML shows that additional oxygen is in a different bonding state to the surface. The concentration dependence of the diffusion coefficient is in agreement with the dependence of Eq.(42) and suggests that the overlayer itself is in a clusterlike configuration which acts as diffusion traps.

An interpretation of the experimental data at coverages below the Stranski–Krastanov layer thickness is not obvious based on the model discussed in this section. A symmetric behaviour around this thickness (with a constant offset due to different diffusion coefficients on both sides) could be proposed based on an analog vacancy model: below c_t the uniform layer would contain diffusing vacancies which aggregate together to form vacancy–clusters in equilibrium with an temperature dependent but concentration independent free vacancy concentration in the two–dimensional layer.

Conclusions

Two independent techniques to obtain information about surface diffusion processes in clustering systems have been described. The analysis of maximum cluster densities in the nucleation regime allows one to separate binding energies and activation energies for diffusion based on a specific model of the actual cluster aggregation.

In the late stage cluster regime the surface diffusion limit

to the mass transport is shown to generally dominate. From growth rates activation energies for clustering are obtained. These data can directly be used to model growth processes. A separation of the surface diffusion contribution to activation energy of clustering is discussed for Stranski–Krastanov growth systems.

Acknowledgements

The author wants to thank L.C. Feldman, M.H. Grabow, J.R. Patel and S. Nakahara (AT&T Bell Laboratories), M. Henzler (University of Hannover, F.R.G.), M.G. Lagally (University of Wisconsin–Madison), W.W. Mullins and W.C. Johnson (Carnegie–Mellon University, Pittsburgh) and J.A. Venables (University of Sussex, England) for valuable discussions.

Financial support by AT&T for a sabbatical stay at Bell Laboratories is acknowledged. Especially thanks are due to L.C. Feldman and B.E. Weir for their hospitality and collaboration during that time.

References

[1] Allen S.M., Cahn J.W. (1979) Microscopic theory for antiphase boundary motion and its application to antiphase domain coarsening. Acta Metall. 27: 1085–1095.

[2] Bauer E. (1958) Phänomenologische Theorie der Kristallabscheidung an Oberflächen. (Phenomenological theory of crystal deposition at surfaces), part I and II. Z. Krist. 110: 372–394,395–431.

[3] Bauer E., Poppa H. (1972) Recent advances in epitaxy. Thin Solid Films 12: 167–185.

[4] Bauer E.G., Dodson B.W., Ehrlich D.J., Feldman L.C., Flynn C.P., Geis M.W., Harbison J.P., Kelley R.D., Matyi R.J., Petroff P.M., Phillips J.M., Peercy P.S., Stringfellow G.B., Zangwill A. (1989) Fundamental issues in heteroepitaxy. Panel report for the Council on Materials Science of the U.S. Department of Energy, Office of Basic Energy Sciences, Division of Materials Sciences (DMS–BES). Copy available from the author.

[5] Becker R., Döring W. (1935) Kinetische Behandlung der Keimbildung in übersättigten Dämpfen (Kinetic treatment of nucleation for supersaturated vapors). Ann. Phys. (5. Folge), 24: 719–752.

[6] Biegelsen D.K., Ponce F.A., Krusor B.S., Tramontana J.C., Yingling R.D. (1988) Graded–thickness samples for molecular beam epitaxial growth studies of GaAs/Si heteroepitaxy. Appl. Phys. Lett. 52: 1779–1781.

[7] Biegelsen D.K., Ponce F.A., Smith A.J., Tramontana J.C. (1987) Initial stages of epitaxial growth of GaAs on (100) silicon. J. appl. Phys. 61: 1856–1859.

[8] Binder K., Stauffer D. (1976) Statistical theory of nucleation, condensation and coagulation. Adv. Phys. 25: 343–396.

[9] Butz R., Wagner H. (1977) Diffusion of oxygen on tungsten(110). Surf. Sci. 63: 448–459.

[10] Butz R., Wagner H. (1979) Surface diffusion of Pd and Au on W single crystal planes. Surf. Sci. 87: 69–84.

[11] Chakraverty B.K. (1967) Grain size distribution in thin films – 1. Conservative systems. J. phys. chem. Solids 28: 2401–2412.

[12] Choi J.Y., Shewmon P.G. (1962) Effect of orientation on the surface self–diffusion of copper. Trans. AIME 224: 589–599.

[13] Crank J. (1975) The mathematics of diffusion, chapter 5. Clarendon, Oxford.

[14] Dunning W.J. (1973) Ripening and ageing processes in precipitates. In: Particle Growth in Suspension (Smith A.L. editor), Academic Press, London, pp. 3–28,61–62.

[15] Feldman L.C., Bevk J., Davidson B.A., Gossmann H.–J., Ourmazd A., Pearsall T.P., Zinke–Allmang M. (1988) Strained layer semiconductor films: Structure and stability. Mat. Res. Soc. Symp. Proc. 102: 405–411.

[16] Feldman L.C., Mayer J.W. (1986) Fundamentals of Surface and Thin Film Analysis, chapters 3 and 5. Elsevier Science Publishers, New York.

[17] Feldman L.C., Mayer J.W., Picraux S.T. (1982) Materials Analysis by Ion Channeling, chapters 1 to 4. Academic Press, New York.

[18] Feldman L.C., Zinke–Allmang M. (1990) Growth and morphology kinetics of adsorbate structures on silicon. J. Vac. Sci. Technol. A 8: 3033–3037.

[19] Frankl D.R., Venables J.A. (1970) Nucleation on substrates from the vapour phase. Adv. Phys. 19: 409–456.

[20] Frenkel J. (1955) Kinetic Theory of Liquids. Dover, New York, p. 422.

[21] Geguzin Y.E., Kaganovsky Y.S., Slyozov V.V. (1969) Determination of the surface heterodiffusion coefficient by the method of mass transfer. J. phys. chem. Solids 30: 1173–1180.

[22] Gibbs J.W. (1876) Trans. Connect. Acad. 3: 108. See: Scientific Papers. (Longmans, Green and Co., New York, 1906), Vol. 1, p. 315.

[23] Gjostein N.A. (1962) Surface self–diffusion. In: Metal Surfaces: Structure, Energetics and Kinetics, chapter 4. Amer. Soc. of Metals, Metals Park, OH, pp. 99–154.

[24] Gomer R. (1983) Surface diffusion – some general remarks. In: Surface Mobilities on Solid Materials (Thien Binh V., editor), Plenum Press, NATO Adv. Study Inst., Series B: Phys., Vol. 86, New York, pp. 1–25.

[25] Gossmann H.–J., Fisanick G.J. (1990) Surface diffusion and islanding in semiconductor heterostructures. Scanning Microscopy 4: 543-553.

[26] Grabow M.H., Gilmer G.H. (1986) Equilibrium and metastable limits to the thickness of coherent epitaxial films. In: Semiconductor-based Heterostructures: Interfacial Structure and Stability (Green M.L., Baglin J.E.E., Chin G.Y., Deckman H.W., Mayo W., Narasinham D., eds.), Metallurgical Soc., Warrendale, PA, pp. 3–19.

[27] Gunton J.D. (1988) Kinetics of ordering in chemisorbed and physisorbed systems. J. Vac. Sci. Technol. A 6: 646–648.

[28] Hanbücken M., Futamoto M., Venables J.A. (1984) Nucleation, growth and the intermediate layer in Ag/Si(100) and Ag/Si(111). Surf. Sci. 147: 433–450.

[29] Harris J.J., Joyce B.A., Gowers J.P., Neave J.H. (1982) Nucleation effects during MBE growth of Sn–doped GaAs. Appl. Phys. A 28: 63–71.

[30] Ishizaka A., Shiraki Y. (1986) Low temperature surface cleaning of silicon and its application to silicon MBE. J. Electrochem. Soc. 133: 666–671.

[31] Katz J.L. (1982) Three dimensional nucleation. In: Interfacial Aspects of Phase Transitions (Mutaftschiev B., editor), Reidel, NATO Adv. Study Inst., Dordrecht, The Netherlands, pp. 261–286.

[32] Kern R. (1982) Three and two dimensional nucleation on substrates. In: Interfacial Aspects of Phase Transitions (Mutaftschiev B., editor), Reidel, NATO Adv. Study Inst., Dordrecht, The Netherlands, pp. 287–302.

[33] Lagally M.G., Kariotis R., Swartzentruber B.S., Mo Y.–W. (1989) Ordering kinetics at surfaces. Ultramicroscopy 31: 87–98.

[34] Lagally M.G. (1990) Scanning tunneling microscopy study of 2–D diffusion, growth, and coarsening in submonolayers of Si on Si(001). In: Kinetics of Ordering and Growth on Surfaces (Lagally M.G., editor), NATO Adv. Res. Workshop Proc. (in press).

[35] Lewis B. (1971) Physical processes in epitaxial growth. Thin Solid Films 7: 179–217.

[36] Lifshitz I.M., Slyozov V.V. (1959) Kinetics of diffusive decomposition of supersaturated solid solutions. Sov. Phys. JETP 35: 331–339.

[37] Lifshitz I.M., Slyozov V.V. (1961) The kinetics of precipitation from supersaturated solid solutions. J. phys. chem. Solids 19: 35–50.

[38] Lupis C.H.P. (1983) Chemical Thermodynamics of Materials, chapters 1 to 3 and 13. North–Holland, New York.

[39] Marqusee J.A. (1984) Dynamics of late stage phase separations in two dimensions. J. Chem. Phys. 81: 976–981.

[40] Naumovets A.G., Vedula Y.S. (1984) Surface diffusion of adsorbates. Surf. Sci. Rept. 4: 365–434.

[41] Neave J.H., Dobson P.J., Joyce B.A., Jing Zhang. Reflection high–energy electron diffraction oscillations from vicinal surfaces – a new approach to surface diffusion measurements. Appl. Phys. Lett. 47: 100–102.

[42] Ostwald W. (1900) Über die vermeintliche Isomerie des roten und gelben Quecksilberoxyds und die Oberflächenspannung fester Körper (The proposed isomery of red and yellow mercury oxides and the surface tension of solids). Z. phys. Chem. 34: 495–503.

[43] Ostwald W. (1920) Grundlagen der Analytische Chemie (Introduction to analytical chemistry), 7th edition. Steinkopff, Dresden (Germany), p. 16–18.

[44] Robinson V.N.E., Robins J.L. (1970) Nucleation kinetics of gold deposition onto UHV cleaved surfaces of KCl and NaF. Thin Solid Films 5: 313–327.

[45] Rogers T.M., Desai R.C. Numerical study of late–stage coarsening for off–critical quenches in the Cahn–Hilliard equation of phase separation. Phys. Rev. B 39: 11956–11964.

[46] Sigsbee R.A. (1971) Adatom capture and growth rates of nuclei. J. appl. Phys. 42: 3904–3915.

[47] Stowell M.J. (1972) Thin film nucleation kinetics. Phil. Mag. 26: 361–374.

[48] Stoyanov S. (1989) A direction of easy diffusion on the (001) face of Ge, Si and III–V semiconductor crystals – how to verify its existence. J. Cryst. Growth 94: 751–756.

[49] Suliga E., Henzler M. (1983) Diffusion of Ag on clean Ge(111) with different step densities. J. Phys. C 16: 1543–1554.

[50] Thomson W. (1870) Proc. Roy. Soc. (Edinburgh) 7: 63 ff. Historic reference, see W.J. Dunning [14].

[51] Thomson W. (1871) Phil. Mag. 43: 448 ff. Historic reference, see W.J. Dunning [14].

[52] Tringides M.C., Wu P.K., Lagally M.G. (1987) Scaling in the ordering kinetics of a chemisorbed overlayer: W(110) – p(2x1)O. Phys. Rev. Lett. 59: 315–318.

[53] van der Veen J.F. (1985) Ion beam crystallography of surfaces and interfaces. Surf. Sci. Rept. 5: 199–288.

[54] Venables J.A. (1973) Rate equation approaches to thin film nucleation kinetics. Phil. Mag. 27: 697–738.

[55] Venables J.A. (1986) Nucleation and growth processes in thin film formation. J. Vac. Sci. Technol. B 4: 870–873.

[56] Venables J.A. (1987) Nucleation calculations in a pair–binding model. Phys. Rev. B 36: 4153–4162.

[57] Venables J.A., Spiller G.D.T., Hanbücken M. (1984) Nucleation and growth of thin films. Rep. Prog. Phys. 47: 399–459.

[58] Volmer M. (1939) Kinetik der Phasenbildung (Kinetics of phase formation). Steinkopff, Dresden (Germany).

[59] Wagner C. (1961) Theorie der Alterung von Niederschlägen durch Umlösen (Theory of ripening of condensates by recrystallization). Z. Elektrochem. 65: 581–591.

[60] Walton D. (1962) Nucleation of vapor deposits. J. Chem. Phys. 37: 2182–2188.

[61] Walton D. Nucleation in liquids and solutions. In: Nucleation (Zettlemoyer A.C., editor), Dekker, New York, pp. 225–308.

[62] White G.M. (1969) Steady–state random walks with application to homogeneous nucleation. J. Chem. Phys. 50: 4672–4678.

[63] Wynblatt P., Gjostein N.A. (1975) Supported metal crystallites. In: Progress in Solid State Chemistry (McCaldin J.O., Somorjai G., editors), Pergamon, Oxford, Vol. 9, pp. 21–58.

[64] Zinke–Allmang M., Feldman L.C. (1988) Concentration dependence of surface diffusion coefficients in clustering systems. Phys. Rev. B 37: 7010–7013.

[65] Zinke–Allmang M., Feldman L.C., Grabow M.H. (1988) Thin film morphology: Equilibrium between clusters

and uniform layers at non–zero temperatures. Surf. Sci. 200: L427–L432.

[66] Zinke–Allmang M., Feldman L.C., Nakahara S. (1987) Role of Ostwald ripening in islanding processes. Appl. Phys. Lett. 51: 975–977.

[67] Zinke–Allmang M., Feldman L.C., Nakahara S. (1988) Initial stages of epitaxial growth: Gallium arsenide on silicon. Appl. Phys. Lett. 52: 144–146.

[68] Zinke–Allmang M., Feldman L.C., Nakahara S. (1990) Three dimensional clustering on surfaces: Overlayers on Si. In: Kinetics of Ordering and Growth on Surfaces (Lagally M.G., editor), NATO Adv. Res. Workshop Proc. (in press).

[69] Zinke–Allmang M., Feldman L.C., Nakahara S., Davidson B.A. (1989) Growth mechanism and clustering phenomena: The Ge–on–Si system. Phys. Rev. B 39: 7848–7851.

[70] Zinke–Allmang M., Gossmann H.–J., Feldman L.C., Fisanick G.J. (1987) Initial stages of interface formation in the Si/Sn system. Mat. Res. Soc. Symp. Proc. 77: 703–708.

[71] Zinke–Allmang M., Gossmann H.–J., Feldman L.C., Fisanick G.J. (1987) Summary abstract: Interface formation in IV–IV heterostructures: Tin on silicon. J. Vac. Sci. Technol. A 5: 2030–2031.

Editor's Note: All of the reviewer's concerns were appropriately addressed by text changes, hence there is no Discussion with Reviewers.